Technical Memo

ECMWF
European Centre for Medium-Range Weather Forecasts

879

Vertical wind shear and convective storms

Tomáš Púčik[1], Pieter Groenemeijer[1]
Ivan Tsonevsky[2]

[1] European Severe Storms Laboratory (ESSL)
[2] ECMWF, Forecast Department

January 2021

Series: ECMWF Technical Memoranda

A full list of ECMWF Publications can be found on our website under:
http://www.ecmwf.int/en/publications

Contact: library@ecmwf.int

Abstract

Convective storms develop in both strong and weak vertical wind shear but long-lived, well-organised convection requires strong vertical wind shear. Studies have shown that the relative frequency of occurrence of convective hazards such as large hail, severe wind gusts and tornadoes increases with increasing vertical wind shear. A particularly strong connection exists between shear and large hail, most pronounced for very large hailstones (≥ 5 cm), which form exclusively in supercells. Likewise, severe wind gusts become more likely with increasing vertical wind shear and with stronger mean flow in the lower troposphere. Tornadoes become more probable with increasing streamwise vorticity and storm-relative helicity near the ground. Excessive rainfall shows the weakest connection to the vertical wind shear. Deep-layer shear, typically measured over a 0–6 km layer, is often used to forecast the most likely convective archetypes (single cells, multicells, linear convection or supercells) in a given situation. Wind shear measured from the surface up to 3 and 1 km AGL are useful for forecasting convective wind and tornado threats, respectively. For tornadoes, 0–1 km storm-relative helicity, which depends not only on speed shear but also on directional shear, is a better predictor for tornadoes than the 0–1 km bulk shear. Numerous composite parameters that incorporate measures of vertical wind shear have been developed. The most robust of those is the product of CAPE (or its square root) and shear, that discriminates well between severe and non-severe convective storms and is one of the ECMWF's Extreme Forecast Index parameters. Hodographs are an important tool for assessing vertical wind shear in different layers. Long, curved hodographs in the lower troposphere represent environments with high values of storm relative helicity conducive to supercells. Recent and ongoing research use environmental parameters, including measures of wind shear, as predictors in statistical models and neural networks to provide probabilistic forecasts of convective hazards. Interestingly, severe weather often happens along the edges of areas with favourable conditions. Another topic of research is the effect of wind shear on the dynamics and physics of storms, including hail growth and the development of damaging gusts, which is being studied intensively using convection-allowing models. Furthermore, recent studies into the predictability of convective storms as a function of wind shear conclude that the evolution and intensity of storms are least predictable when wind shear is weak.

1 Introduction

A convective storm requires three basic ingredients to form: 1) low-level moisture, 2) conditional instability, and 3) lift (Johns and Doswell, 1992; Doswell et al. 1996). The combination of low-level moisture and conditional instability renders an air-parcel buoyant during its ascent. Before the parcel is able to accelerate freely upward from the Level of Free Convection (LFC) where it first becomes positively buoyant, the third ingredient – a lifting mechanism – is required to ensure that the parcel ascends to LFC.

Vertical wind shear, or the change of the horizontal wind vector with height, is not a requirement for a convective storm. In fact, strong vertical wind shear can be a negative factor during storm initiation (Markowski and Richardson, 2010). Wind shear enhances the entrainment of environmental air into an initiating updraught, which reduces its buoyancy and coherence. Increasing updraught tilt also increases

the vertical pressure perturbation gradient force that acts against the buoyancy force. Thus, all other factors being equal, convective initiation is less likely with stronger shear than with weaker shear. However, once a storm has initiated, vertical wind shear plays a different role and can increase its severity and longevity.

The first speculations of the relevance of wind shear on severe weather can arguably be credited to Wegener (1928) who noted that the formation of tornadoes would likely involve tilting of vortices (Antonescu, 2016), corroborated by observations like those of Van Everdingen (1925) who noted exceptionally strong winds measured by a kite at approximately 1500 m on the same day that a violent tornado struck the eastern Netherlands.

Several studies in the 1950s, 1960s and 1970s recognized the influence of shear on the behaviour of convective storms (Newton, 1960; Browning 1964) and the association of strong vertical wind shear with severe weather, such as tornadoes, large hail, and severe wind gusts (Maddox, 1976). Chisholm and Renick (1972) presented composite vertical wind profiles associated with three main thunderstorm archetypes: single cells, multicells and supercells (Figure 1). Multicell storms are storms regenerated by new updraught pulses, or storm cells, that are triggered on the flanks of older cells. Supercells are persistent storms that exhibit updraught rotation, i.e. a mesocyclone, and very often produce severe weather. Their understanding was that single cells form in weak vertical wind shear, whereas stronger shear was associated with multi- and supercells. The difference between the latter two was that the shear was unidirectional for multicells, while it changed in a clockwise direction with height for supercells.

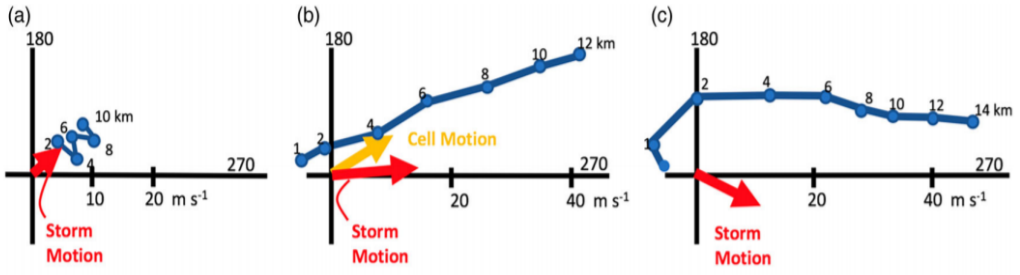

Figure 1. Composite hodographs associated with a) single cells b) multicells and c) supercells according to Chisholm and Renick (1972). Figure modified by Sills and Joe (2019). See Chapter 3.3 for more information about hodographs. Figure licensed under a CC BY-NC-ND 4.0 license.

During the 1970s and 80s, numerical modelling studies using idealised cloud models have greatly advanced our understanding of how wind shear influences the morphology of convective storms. Pioneering research in this direction was done by Klemp and Wilhelmson (1978), Wilhelmson and Klemp (1978), and Weisman and Klemp (1984). These studies provided the physical explanation for the deviant storm motion of supercells, for storm-splitting, and for updraughts being both longer-lived and stronger in environments with strong wind shear. Davies-Jones (1984) provided a mathematical description of how updraught rotation arises in supercells and related this to the helicity of the flow. Helicity is the extent to which a corkscrew-like motion occurs and has become a frequently used quantity in forecasting severe convective storms (Davies-Jones et al. 1990).

While these studies mostly concentrated on the dynamics of supercell convection, an important study on multicells was done by Rotunno et al. (1988), who, using a set of numerical simulations, found that long-lived squall lines require a state of balance between perturbation pressure gradient forces induced by cold pool and the ambient vertical wind shear. This is commonly referred to as "RKW-theory", after the initials of the article's authors. While some of the presented conclusions have been disputed in the literature (e.g., Coniglio et al. 2006), it has upheld its relevance in explaining how shear at the depth of the gust front contributes to deeper lift of the parcels ahead of it, and thus to the regeneration of convective system (Bryan et al. 2006).

2 The impact of wind shear on convective storms and hazard type

2.1 The effect of wind shear on convective storms

The most important effect that wind shear exerts on convective storms is the prolongation of their life span beyond the typical life of a single cell in the absence of wind shear. Single cells usually last 45 – 60 minutes, while their mature stage typically lasts only 15-20 minutes. The lifespan of a single cell is limited by the collapse of its precipitation core, that is filled with heavy hydrometeors, onto its updraught, and by undercutting of the updraught from its source of potentially buoyant air by cold outflow driven by the evaporation of precipitation. Vertical wind shear increases a storm's longevity by counteracting these two detrimental processes (Markowski and Richardson, 2010).

2.1.1 Separation of updraught and downdraught and storm-relative winds

Stronger vertical wind shear implies that strong storm-relative winds may occur, in particular at higher altitudes. Mid- and upper-level winds can advect the precipitation away from the updraught tower, such that the outflow produced by evaporational cooling of this precipitation does not undercut the inflow into the storm. At the same time, the lower tropospheric storm-relative wind (inflow) can limit the motion of cool outflow air away from the updraught, which prevents it from being undercut early. In addition, stronger inflow into a storm is also associated with wider and stronger updraughts (Peters et al., 2019).

2.1.2 Perturbation pressure forces

Vertical wind shear results in the development of an upward vertical pressure perturbation gradient force within the storm or at the flank of the storm. Such forces lift new air to its Level of Free Convection, thereby regenerating and potentially enhancing the updraught. The pressure perturbation gradients may either force the initiation of new cells along the gust front of a storm (Figure 2) – specific for multicells and squall lines – or underneath a low pressure perturbation that develops within or next to the updraught core – this occurs in supercells. An upward pointing pressure perturbation gradient forces air to its LFC and thus ensures the persistence of the storm. The often visually stunning appearance of some supercells with smooth, laminar-looking cloud bases actually results from this forced ascent of parcels while they are still denser than the surrounding air (Figure 4).

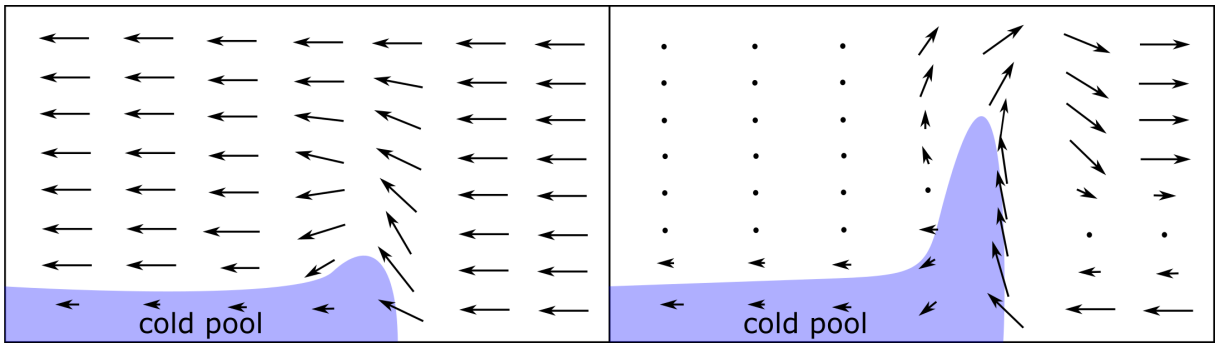

Figure 2. An idealized simulation of a cold-pool relative flow in the absence of shear (left) and in the case that cold pool and shear are balanced (right). Deeper lift along the edge of the cold pool is generated in the balanced state on the right.

Figure 4. Supercell cloud base with laminar – rather than buoyant – look and a tail cloud. Photographed by Pieter Groenemeijer.

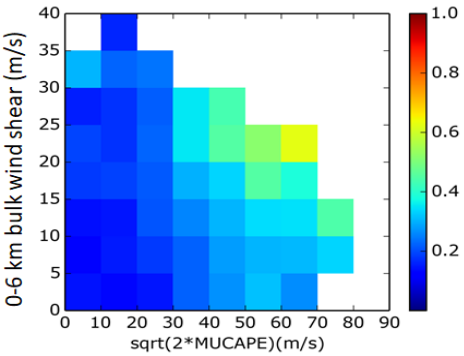

Figure 3. Relative frequency of severe convective storms in the CAPE and 0–6 km bulk shear parameter space. Adapted from: Púčik et al. (2015).

Thus pressure perturbation gradients may accelerate updraughts beyond the speeds that would result from buoyancy alone (Weisman and Klemp, 1984). The strongest updraughts and downdraughts in convective storms occur with strong vertical wind shear and substantial CAPE (Kirkpatrick et al., 2009). Besides the longevity and strength of updraughts, their width is also increased by shear, as found in the recent studies by Dennis and Kumjian (2017), Trapp et al. (2017), Marion and Trapp (2019) and Peters et al. (2019). The cores of wider updraughts are more protected from entrainment and thus tend to be stronger than narrow updraughts (Peters et al. 2019). Furthermore, wider updraughts are typically more continuous or plume-like, in contrast to narrower updraughts that are more intermittent, consisting of a series of subsequent buoyant bubbles.

Because vertical wind shear increases the lifetime of convective storms as well as the speed and width of up- and downdraughts, the severity of severe convective storms increases with increasing shear. Indeed, a strong correspondence between the relative frequency of severe convective storms and vertical wind shear has been confirmed over the U.S.A., Europe and Australia (Craven and Brooks 2004; Brooks 2009, Allen and Karoly 2014, Púčik et al. 2015, Taszarek et al. 2017). Figure 3 shows the increasing probability of severe weather over Central Europe. The link between vertical wind shear and individual hazards of severe convective storms, such as large hail, severe wind gusts, tornadoes and excessive rainfall, is more complicated.

2.2 Wind shear and convective hazards

2.2.1 Large hail

Brooks (2013) and Púčik et al. (2015) found that of all severe weather threats, large hail depends most strongly on high CAPE and strong shear between the surface and the mid-troposphere, e.g. between 0 and 6 km above ground level. This is because large hail requires strong, wide, and persistent updraughts (Nelson 1987) all of which are favoured by high CAPE and strong shear. In fact, very large hail exceeding 5 cm in diameter is almost exclusively produced by supercells (Smith et al. 2012; Blair et al. 2017). Supercells are convective storms with a persistent, deep mesocyclone, i.e. a circulation with a depth of typically 2 – 10 km, that can be detected by Doppler radar. Some studies have found that vertical wind shear is a better hail size discriminator than CAPE (Berthet et al. 2013, Johnson and Sugden 2014) or that CAPE alone is a poor discriminator of hail size (Edwards and Thompson 1998). For smaller hail sizes (< 2 cm), strong vertical wind shear is not required, and buoyancy-related parameters may work better as hail predictors (Manzato 2012). While very large hail requires strong vertical wind shear, small variations in the vertical wind profile can strongly influence hail embryo trajectories through a storm's updraught (Dennis and Kumjian, 2017). As a result, seemingly similar environments may produce a wide range of hail sizes.

2.2.2 Severe wind gusts

The relation between severe wind gusts and vertical wind shear is more complicated than for large hail. Isolated strong downdraughts leading to severe winds near the surface, i.e. downbursts, depend primarily on water loading within the storm, the environmental lapse rate (i.e. the vertical temperature gradient), and lower tropospheric relative humidity (Srivastava 1985) and not as much on wind shear. As a consequence, downbursts may also occur with weak vertical wind shear.

Longer-lived and more widespread convective windstorms are often tied to the deep cold pools and mesoscale circulations created by linear mesoscale convective systems, i.e. squall lines. Bow echoes, a subset of squall lines named after their appearance on weather radar, have been associated with the most damaging convective windstorms (Przybylinski 1995; Gatzen 2013, Taszarek et al., 2019). Numerical simulations of bow echoes by Weisman (1993) showed that strong vertical wind shear in the lower troposphere is required for their formation. Although Evans and Doswell (2001) have shown that bow echoes have also occurred with a "lower-than-ideal" amount of wind shear, more recently it was confirmed that the most intense convective windstorms were associated with the strongest wind shear (Cohen et al. 2007).

Besides the strength of the shear, the orientation of mean flow with respect to the convective system, or the air-mass boundary along which it initiated – typically a zone with convergent wind near the surface – is important (Kuchera and Parker 2006, Corfidi 2003): fast-moving convective windstorms are more likely when the mean tropospheric flow is perpendicular to the orientation of the squall line.

2.2.3 Tornadoes

Tornadoes can be divided into two groups: mesocyclonic and non-mesocyclonic. Non-mesocyclonic tornadoes form by stretching pre-existing vertical vorticity by the updraught of a convective storm (Wakimoto and Wilson 1989; Brady and Szoke 1989; Davies 2006; Markowski and Richardson 2010), which typically happens along a boundary across which the low-level wind changes direction. This

process does not require strong vertical wind shear. Because this type of tornado depends on the presence of small-scale boundaries, non-mesocyclonic tornadoes are comparatively hard to forecast.

In mesocyclonic tornadoes, vorticity is stretched by a parent mesocyclone. Thus, the first step in forecasting mesocyclonic tornadoes is to identify whether a supercell can form. However, most supercells never produce a tornado (Trapp et al. 2005). A myriad of field experiments, observational and numerical modelling studies (e.g., Markowski and Richardson 2014) were devoted to the discrimination between non-tornadic and tornadic supercells. It was found that the height of the cloud base and the magnitude of the vertical wind shear across the lowest 1 km were skilful discriminators (Thompson et al. 2003, Craven and Brooks, 2004, Grams et al. 2012). The probability of tornadoes increases both with lower cloud bases and with stronger low-level wind shear.

Recent studies show that the characteristics of the wind profile in the lowest hundreds of meters may be the most important for determining whether vortex stretching from the parent mesocyclone will be sufficient for forming a tornado (Coffer and Parker 2017). Coffer et al. (2019) recently showed that the shear in the lowest 500 m was an even more skilful predictor of tornadoes than shear in the lowest 1000 m. While the shear in the lowest hundreds of meters may be the best discriminator, it is also very sensitive to very local variations of flow in the boundary layer that may not be resolved by radiosondes or be confidently predicted in a deterministic sense by numerical weather prediction models. Studies using radiosonde-based observations over Europe (Púčik et al. 2015, Taszarek et al. 2017) showed little added value in using 0-1 km shear rather than 0-3 km shear when discriminating between non-tornadic and significantly tornadic (F2+) environments.

2.2.4 Excessive rainfall

Of all severe weather hazards, excessive rainfall is the one that is least linked to the presence of strong vertical wind shear. An important factor for excessive rainfall occurrence is precipitation efficiency, defined as the ratio of the mass of water falling as precipitation to the influx of water vapor mass into the storm cloud (Doswell et al. 1996). The other important factors are the influx of water vapor and the duration of the precipitation.

Marwitz (1972a), showed that precipitation efficiency was negatively correlated with wind shear in storms across the United States High Plains, possibly due to increased entrainment into the updraught and subsequent evaporation of hydrometeors, but a number of subsequent studies have not been able to corroborate this (Trudeau and Zawadzki, 1983; Fankhauser 1988). Another reason why shear may be considered detrimental for excessive rainfall accumulations is that storms often travel faster in environments of stronger shear. However, convective storms may remain quasi-stationary even in strong flow if new cells keep forming at the upwind flank of the system, a process called back-building (Corfidi et al. 1996). Storms that develop in strong wind shear tend to have stronger updraughts and wider updraughts with a stronger moisture influx. Hitchens and Brooks (2013) found that supercells typically produce more intense precipitation than non-supercells. Idealized numerical model simulations showed that in a moist environment with high relative humidity throughout the troposphere, the dynamical contribution to the updraught from a mesocyclone increased precipitation rates (Nielsen and Schumacher 2018). The net effect of wind shear on heavy precipitation is ambiguous and is likely not the same for all geographical regions and all meteorological situations.

3 Vertical wind shear parameters

There are numerous different measures of vertical wind shear in use by forecasters and researchers. Most straightforward is the literal calculation of vertical shear of the horizontal wind, i.e. a velocity difference divided by depth, which yields a unit of s^{-1}. More commonly the magnitude of the vector wind difference between two fixed levels is used, in particular by the forecasting community, and this is called “bulk shear”, “bulk wind shear” or “bulk wind difference”. Ordinarily, computations of such a parameter do not involve division by the depth of the layer across which the shear is considered.

3.1 Bulk wind shear

A common layer over which the bulk shear is calculated is that from 0 to 6 km above the ground, where the 0 km is usually meant to mean the wind at 10 m, the standard WMO measuring height, or, occasionally in some studies, an average over the lowest 500 m. This wind difference is often simply referred to as deep-layer shear, abbreviated in technical forecast discussions by DLS. The 0–6 km layer has been found to discriminate well between non-supercell and supercell convection (Rasmussen and Blanchard 1998, Thompson et al. 2003) and has been used in many proximity sounding studies of severe convective storms (e.g., Púčik et al. 2015; Taszarek et al. 2017). The choice of 0–6 km is arbitrary and was likely chosen as a surrogate to the standard pressure level of 500 hPa. Houston et al. (2008) investigated the skill of different bulk shear depths in discriminating non-supercell from supercell environments: they found little variation in skill for layers extending from 0 up to 4, 5, or 6 km.

Supercells become more likely as the 0–6 km bulk shear approaches and exceeds 20 m/s (Table 1). There is, however, no absolute threshold value. Single cells are typical for values below 10 m/s, while increasingly well-organized multicell storms tend to occur when DLS rises from 10 to 20 m/s. Doswell and Evans (2003) found that derechoes, large-scale convective windstorms that are usually associated with well-organized linear convective systems, typically occur with strong vertical wind shear, similar to supercells. A strongly sheared environment favours both supercell convection and derechoes. In fact, derechoes frequently evolve from one or more isolated supercells (e.g. Taszarek et al. 2019). The process responsible for this is not a result of changing wind shear, but the clustering of convective cells along a common outflow boundary. This happens most frequently when widespread initiation has occurred along a common initiating boundary. In that case, the downdraughts of individual storms that result from hydrometeor evaporation will often merge into one common pool of cold air (Dial et al. 2010). The edge of the resulting large and deep cold pool then often becomes the focus for new cell initiation, thereby enhancing the multicellular, rather than supercellular, character of the convective developments.

0–6 km shear:	< 10 m/s	8 – 20 m/s	> 18 m/s
convective mode:	**single cells**	**multicells**	**supercells**
system propagation:	gust front unable to initiate new cells, at least in any organized way; convection is short-lived	gust front initiates new cells repeatedly (downshear flank preferred in a homogeneous environment); system propagation is driven by gust front lifting	updraughts may be quasi-steady; propagation governed by vertical pressure gradients extending over a deep layer rather than by gust front lifting

Table 1. Main convective archetypes, their basic dynamic traits and link to the magnitude of 0–6 km bulk shear, according to Markowski and Richardson (2010).

While the nature of the lifting process is an important factor determining whether multicellular and supercellular convection develops in strongly sheared environments, there are some traits of the wind profile that are more typical for supercells, and some that are more typical for linear convective systems. Most importantly, supercells tend to have shear distributed over a deeper layer (Weisman and Klemp, 1986; Doswell and Evans 2003; Bunkers et al. 2006). Meanwhile linear systems thrive when strong shear is confined to the bottom kilometres of the troposphere, which results in weak mid- to upper tropospheric winds, precipitation fall-out to the rear part of the storm and thus deepening of the cold pool (Markowski and Richardson 2010). Three layers of the bulk shear are most commonly considered for forecasting severe convective storms.

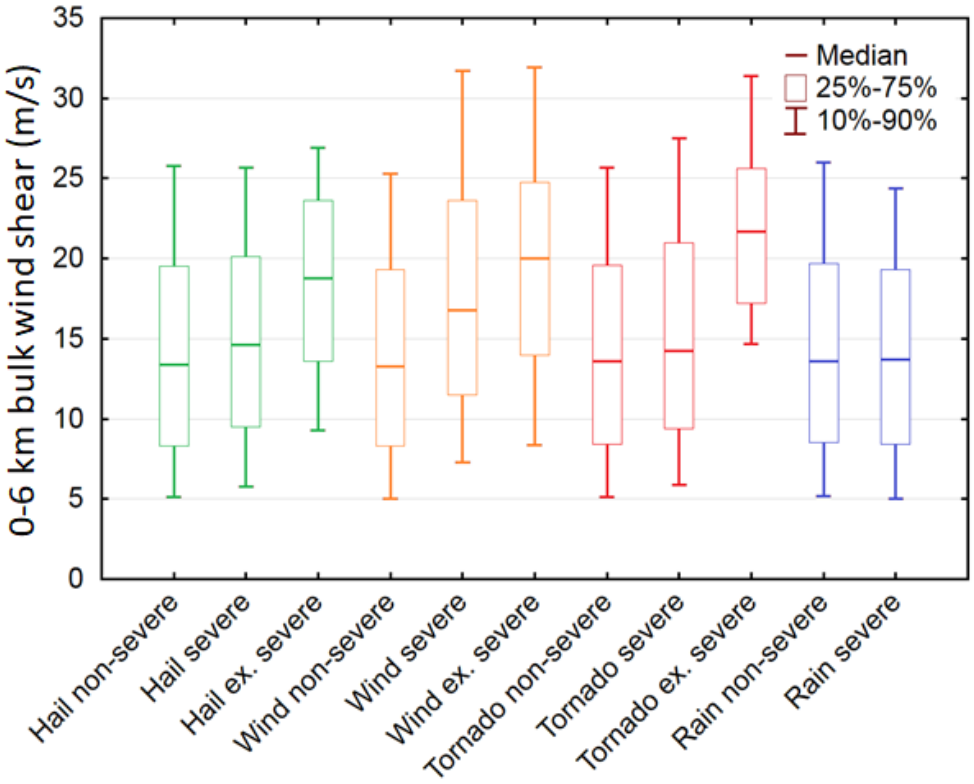

Figure 5. Box plot of distribution of 0–6 km bulk wind shear values in different types and severities of convective storm hazards. From Púčik et al. (2015).

0 – 6 km layer

- used for convective type forecasting, especially non-supercells vs supercells
- discriminates well between environments of hail of 2–5 cm and ≥ 5 cm (supercells required for hail ≥ 5 cm)
- discriminates well between environments of non-severe, severe (25–32 m/s) and extremely severe (≥ 32 m/s) wind gusts
- the relative frequency of large hail, severe wind gusts and tornadoes increases with an increased product of CAPE and 0–6 km bulk shear

Across Europe, almost all events with hail ≥ 5 cm, wind gusts ≥ 32 m/s and F2+ tornadoes occur with 0–6 km bulk shear > 15 m/s (Figure 5, from Púčik et al. 2015).

0–3 km layer

- used for mesoscale convective system and convective windstorm forecasting
- in cases of strong shear > 15 m/s that is confined to the lower troposphere, expect storms to favour transitioning into line segments, rather than staying as isolated supercells.

- discriminates well between environments of non-severe, severe (25 - 32 m/s) and extremely severe (≥ 32 m/s) wind gusts

also discriminates well between environments in which significant tornadoes (≥ F2) occur vs. those that lead to weak (< F2) or no tornadoes.

0–1 km layer

- used for tornado forecasting given that supercells occur; values above 10 m/s are supportive of mesocyclonic tornadoes

None of these bulk shear parameters discriminate well between convective storms with and without subsequent flash flooding.

3.2 Storm-relative winds

Storm-relative winds are the winds relative to the motion of the convective storm. Ground- and storm-relative winds may differ substantially. In order to calculate storm-relative winds, a storm motion vector needs to be calculated. Typically, ordinary cells move with the mean wind in the lower to mid-troposphere (e.g. 0–6 km). More information on the storm motion vector calculation is provided in the next section on hodographs.

Larger vertical wind shear usually implies stronger storm-relative winds. While storm-relative winds are not very commonly used in severe convective storm forecasting, several studies have pointed out that stronger inflow to storm in the lower troposphere (up to 3 km above the surface) is associated with more severe storms (Kerr and Darkow, 1996; Thompson 1998). Recently, numerical modelling studies found that stronger inflow leads to wider and stronger updraughts and more latent heat release within the convective storms (Alfaro 2017; Peters et al. 2019a, 2019b).

Tornadic supercells have stronger mid-tropospheric storm-relative winds (calculated over the height interval of 4–6 km) than non-tornadic supercells (Thompson 1998). Brooks et al. (1994) associated weaker mid-tropospheric storm-relative winds with higher precipitation in the rear-flank downdraught of the storm and with a stronger outflow that eventually undercuts the updraught. In fact, a study on supercells producing extreme wind gusts at the surface, but no tornadoes, found out that such storms featured very weak mid-tropospheric storm-relative flow (Brooks and Doswell 1993).

Upper tropospheric storm-relative winds are typically calculated for altitudes above 8 or 9 km. There are some indications that stronger upper tropospheric storm-relative winds are associated with storms that have a lower precipitation efficiency and with longer lasting supercells (Rasmussen and Straka 1998, Bunkers et al. 2006).

3.3 The hodograph, storm relative wind and helicity

3.3.1 Hodograph

Vertical wind shear can be assessed using the vertical wind profile that is often plotted next to and aligned with a thermodynamic diagram. This is often done simply by displaying a number of wind barbs or wind vectors at various altitudes. Forecasters often use them to extract whether the shear is mostly speed shear, directional shear, or both, and subsequently determine the most likely convective type. This

process is not very straightforward, as it is difficult to visually derive bulk shear numbers from barbs, let alone more complicated metrics such as storm-relative helicity, discussed below. Storm-relative helicity is often thought to be associated with winds veering with height, something that can easily be derived from a number of barbs, but this is not always the case.

A hodograph (Figure 6) is a helpful tool to assess the change of the wind and the wind shear vector with height. It is obtained by drawing multiple wind vectors from the origin of a coordinate system along the direction into which the wind blows while the arrow length represents the wind speed: the hodograph is then the line that connects the tips of the wind vectors, for sequentially increasing altitudes. The wind shear vector (i.e. the vertical derivative of the horizontal wind vectors) aligns along the tangent to this curve whilst the length of the hodograph between two altitudes represents the magnitude of the wind shear. Along a curved hodograph, the wind direction changes with height, but – and this is important for the dynamics of storm systems – the shear vector changes with height as well.

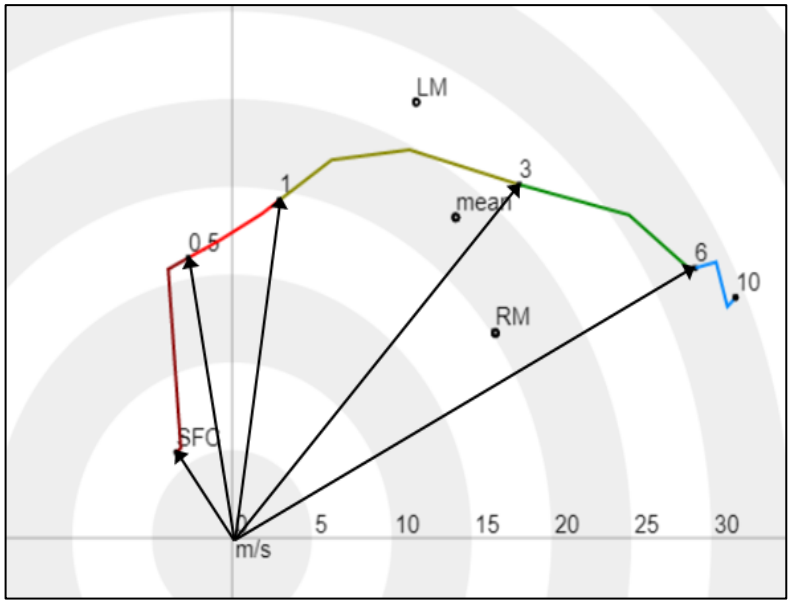

Figure 6. A hodograph with the colours of the hodograph line representing different vertical layers. Wind vectors are plotted for surface (SFC), 0.5, 1, 3 and 6 km AGL wind. Storm motion is plotted for ordinary cells (mean), left-moving (LM) and right-moving (RM) supercells. Further details about LM and RM supercells and wind shear can be found in section 3.3.3.

3.3.2 Storm-relative wind

Storm-relative winds can be easily read from the hodograph, once the storm motion is known. The motion of ordinary cells can be estimated using a pressure weighted mean wind in the lower to mid-troposphere (typically from surface up to 6 km). Storm-relative winds at a given altitude are then found by vectors from the point representing the storm motion to the hodograph at that altitude.

The curvature of the hodograph throughout the lower troposphere, typically the bottom 3 km, is of interest as it represents the layer from which air flows into to the storm's updraught(s). The rotation in a supercell arises as horizontally oriented vorticity, that exists because of the vertical wind shear, is tilted and stretched by the updraught of a convective storm. Figure 7 gives two examples where the shear in

the lowest 0.5 km, i.e. the stretch of the hodograph between 0 and 0.5 km (brown) is approximately parallel (left) or perpendicular (right) to the storm-relative wind. Here, the storm is assumed to behave and move as a "right-moving" (RM) storm. The vorticity vectors (purple) that are perpendicular to the low-level shear are perpendicular (left) and parallel (right) to the storm-relative wind. The vorticity in that layer of air is said to be crosswise (left) or streamwise (right), respectively.

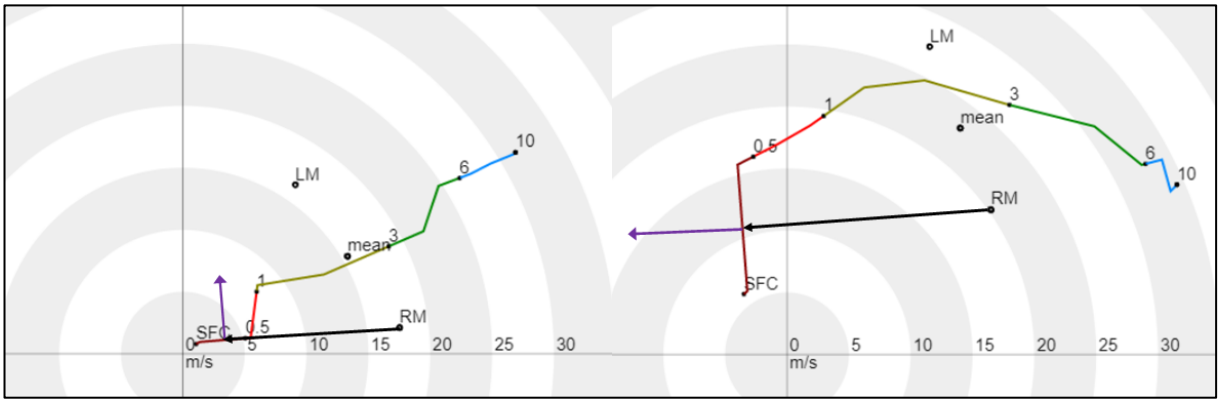

Figure 7. Hodographs showing the storm-relative inflow winds for 0–0.5 km above ground level (black) and the vorticity vector (violet) in the same layer. In case of the left hodograph, the vorticity is almost purely crosswise in this layer, whereas it is almost purely streamwise in the example on the right.

In the case of purely crosswise vorticity, the updraught tilts the vorticity in a way that results in maxima on the updraught's flanks but no net rotation arises within the updraught. In the streamwise vorticity case, the maximum of vorticity after tilting would be collocated with the updraught maximum implying that the updraught as a whole will rotate.

3.3.3 Storm-relative helicity

Thus, the orientation of the vorticity vector with respect to the storm-relative inflow vectors is important for anticipating the degree of rotation in the convective storms, i.e. the potential for supercell convection. In order to achieve updraught rotation, the storm motion must not lie on the hodograph. The greatest degree of streamwise vorticity can be expected when the hodograph is both long (allowing for strong storm-relative inflow) and strongly curved (allowing for streamwise vorticity) as in Figure 7 (right). Storm-relative helicity is a measure that expresses this quantitatively (Davies-Jones, 1984). Helicity is the extent to which a fluid follows a corkscrew-like motion. This is the case when the vorticity is aligned with the velocity in the fluid, in other words, helicity is the dot product of the wind vector and vorticity vector.

The helicity relevant to the generation of rotation in a convective storm must be calculated using a storm-relative wind profile, where any vertical wind components are ignored, this is called **storm-relative helicity (SRH)**:

$$SRH = -\int_0^h \hat{k} \cdot (\vec{v} - \vec{v}_{storm}) \times \frac{d\vec{v}}{dz} dz$$

where $\vec{v} - \vec{v}_{storm}$ is the storm relative wind, $d\vec{v}/dz$ is the vertical wind shear and $\hat{k}$ is the unit vector in the upward direction.

The helicity is integrated over the depth (h) of the inflow to the storm, which is conventionally approximated over the depth of the bottom 3 km (Davies-Jones et al. 1990) or 1 km (Thompson et al. 2003). For tornado forecasting, a layer as shallow as 500 m has been proposed (Coffer et al. 2019). On the hodograph, storm-relative helicity is proportional to twice the area swept out by the storm-relative wind vectors at the ground, at the 3 km above the ground and the hodograph line (Figure 8). This area increases with increasing hodograph length, with increasing curvature and also with the storm motion vector lying further away from the hodograph.

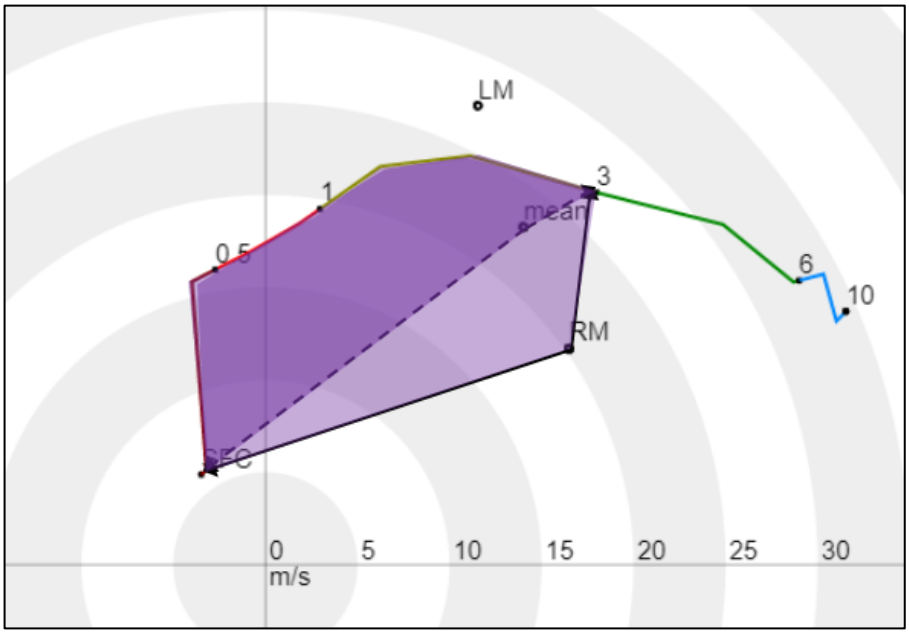

Figure 8. A curved hodograph with the storm-relative wind at the surface and at 3 km AGL for ordinary cell motion (mean, dashed arrows) and right-moving supercell (RM, full arrows). The storm-relative helicity (SRH) corresponding to ordinary cell motion is proportional to the size of the dark violet area, whereas SRH corresponding to the right moving supercell is proportional to the sum of the dark and light violet areas.

Forecasters often require high values of SRH or curved hodographs to call an environment conducive to supercells. However, as Weisman and Rotunno (2000) note, the basic process through which a storm attains supercellular characteristics (tilting and stretching of vorticity) can occur both with linear and curved hodographs. In case of a linear hodograph, vorticity centres that form on the flanks of the updraught will force new updraughts on the sides of the storm. This will result in a storm splitting into a left-moving (LM) and right-moving (RM) storm that both propagate away from the original storm motion vector. After this split, the storm motion vector will lie outside of the hodograph even if it is straight (Figure 9).

Because storms in strongly sheared environments tend to have a significant component of motion because of a preferred development on one side of the storm, SRH is typically calculated taking this deviant motion into account. The SRH that forecasters often see displayed is usually the helicity

available to the storm once it already evolved into a (super)cell with such a deviant motion. For this reason, deep-layer shear discriminates better between supercells and non-supercells than the SRH (McCaul and Weisman 2001, Nowotarski and Jensen 2013, Peters et al. 2020). Typically, SRH will be calculated for the right-moving supercells in the Northern Hemisphere. This is because the vertical wind profile usually favours right-moving over left-moving supercells as a result of the typical veering of winds with height in the boundary layer in the Northern Hemisphere. This veering with height is a characteristic of the Ekman spiral, the wind profile that results from the assumption that within the boundary layer a balance exists between the pressure gradient force, the Coriolis force and turbulent friction. For the Southern Hemisphere, SRH is usually calculated for left-moving supercells, since the wind usually backs with height as a result of the opposite direction of the Coriolis force.

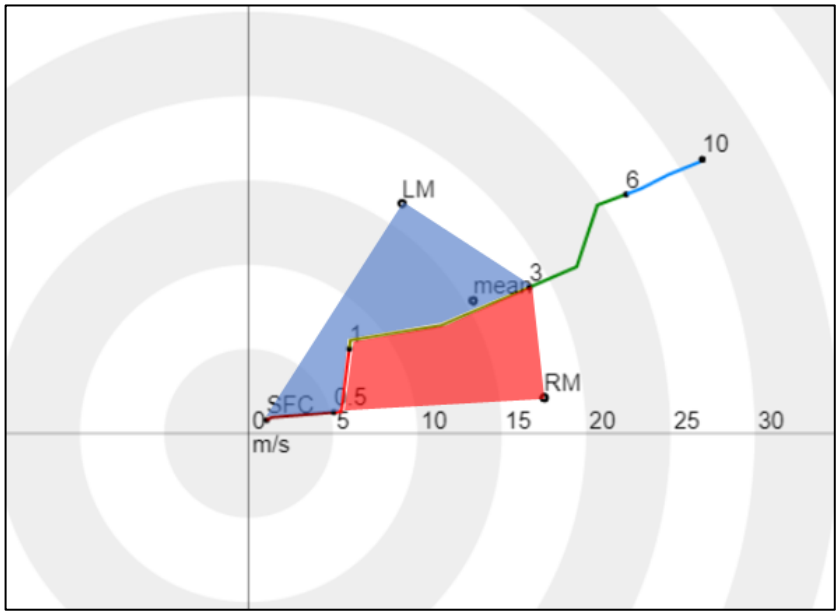

Figure 9. A straight hodograph with areas of storm-relative helicity for left-moving (blue, LM) and right-moving (red, RM) supercells.

SRH calculation requires a correct anticipation of the storm motion vector. The empirical *Internal Dynamics method*, or simply *ID-method*, was proposed by Bunkers et al. (2000) and uses the mean wind in the lowest 6 km and the shear vector between the average winds at 0-0.5 km AGL and 5.5-6 km AGL (Figure 10). First, the mean wind is used to estimate the motion of an ordinary cell and the deviant propagation of supercells is set to be 7.5 m/s to the left and right of the mean wind along the line perpendicular to the shear vector. This technique is empirical and does not account for the effects of cold pool, orography or boundaries on storm propagation (Bunkers et al. 2000). It was shown to produce largest errors in environments of fast storm motion, very high SRH, low relative humidity in the low to mid-troposphere or high CIN (Bunkers 2018). The Internal Dynamics method cannot be applied to the movement of mesoscale convective systems, where propagation is usually predominantly driven by the effects of the cold pool (Corfidi 2003).

SRH best applies to supercell convection and thus should not be used to forecast the intensity of multicellular convection, including squall lines and bow-echoes. Once the deep-layer shear is strong enough for supercells, SRH can be used to anticipate the strength of low-level rotation within the

supercell. Other storm characteristics, such as the updraught strength or updraught width are better characterised by bulk wind shear (Peters et al. 2020). The strength of low-level rotation seems to be important especially for tornadoes (Thompson et al. 2003, Grams et al. 2012). For tornado forecasting, calculating SRH over the shallower layers (0–500 m or 0–1000 m) may yield better results than using the layer of 0–3 km (Nowotarski and Jensen 2013, Coffer et al. 2019). Over the U.S.A., SRH values over 250 m^2/s^2 in the 0–3 km layer and over 100 m^2/s^2 in the 0–1 km layer were associated with tornadoes, increasing with increasing tornado intensity (Anderson-Frey et al. 2016). Over Europe, tornadoes were observed with lower values of SRH (Púčik et al. 2015; Taszarek et al. 2017).

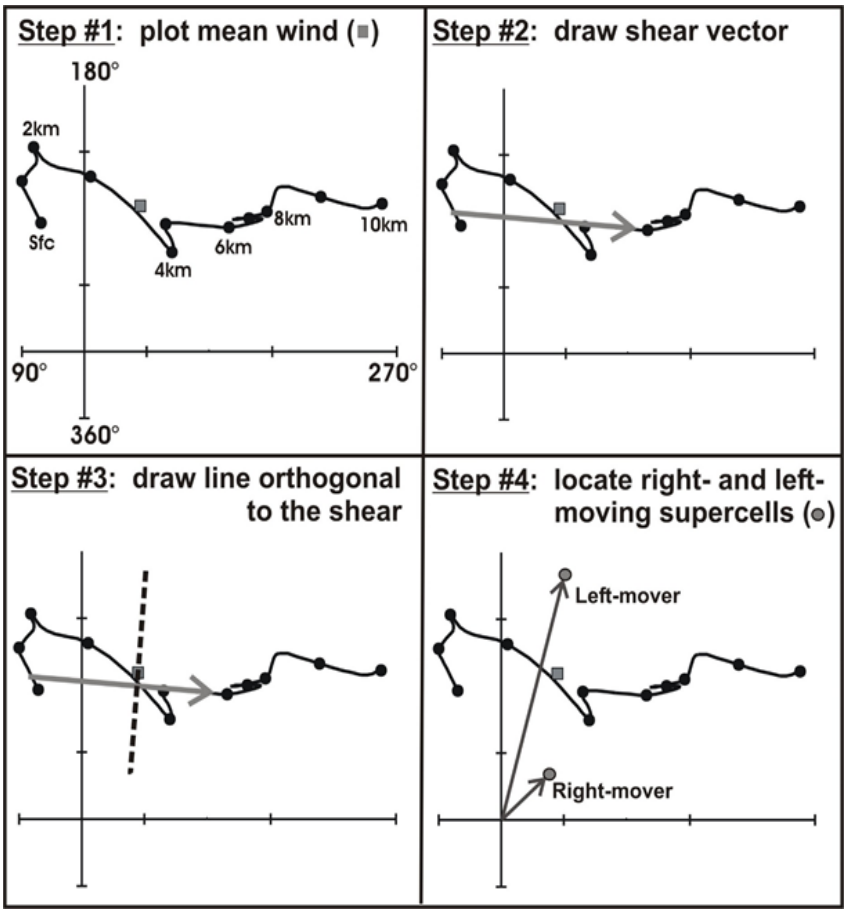

Figure 10. Construction of storm motion vectors using the Bunker's ID-method (Bunkers, 2000). Image courtesy of Matthew Bunkers.

The correlation between other convective hazards and SRH is low. While supercells are prolific large hail producers, Dennis and Kumjian (2017) even found decrease in the hail production in simulated supercells when increasing the SRH in the environment. Thus, SRH should be used predominantly for tornado forecasting. The shape of the hodograph can be then used to infer the characteristics of supercells. Straight, long hodographs will produce mirror-image splitting supercells while curved hodograph will favour either left or right-split of the pair. Curved hodograph with wind veering with height will favour right-moving supercells, whereas curved hodograph with wind backing will favour the left-movers.

4 Composite parameters including measures of vertical wind shear

4.1 Effective shear and effective storm-relative helicity

Effective bulk shear and **effective SRH** are measures of vertical wind shear that take the thermodynamic profile of the troposphere into consideration. Conventional measures of bulk shear and SRH are typically calculated over a constant depth, e.g. 0–6 km for bulk shear and 0–3 km for SRH. Here, 0–6 km is approximately a half of the height of a typical convective storm and the 0–3 km can be thought of the layer of air from which rising parcels in the updraught originate. In practice, of course, low topped convection in winter may not even be 6 km tall, while the storms near the equator can reach as high as 18 km. Furthermore, it is assumed that the base of the inflow layer to the storm is near the ground, which is not true for elevated storms, i.e. storms with an inflow layer substantially above the ground. To account for the varying heights of the inflow layer and storm heights found in various situations, Thompson et al. (2007) defined *effective* shear and *effective* storm-relative helicity by computing them for an inflow layer in which parcels have CAPE of at least 100 J/kg and CIN less than 250 J/kg: effective SRH is calculated by integration over the layer satisfying these conditions, while effective bulk shear is calculated as the difference between the wind at the bottom of the inflow layer and that halfway between the distance from the inflow layer to the equilibrium level. They found that these varieties of SRH and bulk shear discriminated better between non-supercells and supercells than their conventional fixed-layer equivalents.

Figure 11 illustrates a situation where effective SRH and effective bulk shear are very different from their conventional fixed-layer equivalents. The model predicted very high values of bulk shear (exceeding 30 m/s in the 0–6 km layer) and SRH (over 400 m^2/s^2) over the Netherlands. However, the boundary layer was stable and parcels originating from the surface would have zero CAPE. The inflow layer to the storms was situated above the boundary layer, at around 850 hPa in the shown profile. The strong vertical wind shear below this altitude would be ineffective in the sense that it does not affect the organization of the convection because these parcels would not participate in the convective overturning. Calculating the effective bulk shear for the given profile would yield approximately 13 m/s, much less than the 0–6 km value of 30 m/s.

It is important to note that, while effective forms of bulk shear and SRH may be superior to their ordinary forms, they only work well provided that the temperature and humidity profiles are simulated correctly. Potential inaccuracies of these profiles will negatively impact the accuracy of the shear parameter. Whenever – perhaps incorrectly – no CAPE is diagnosed, both the effective bulk shear and the effective SRH will be zero, even if vertical wind shear is strong.

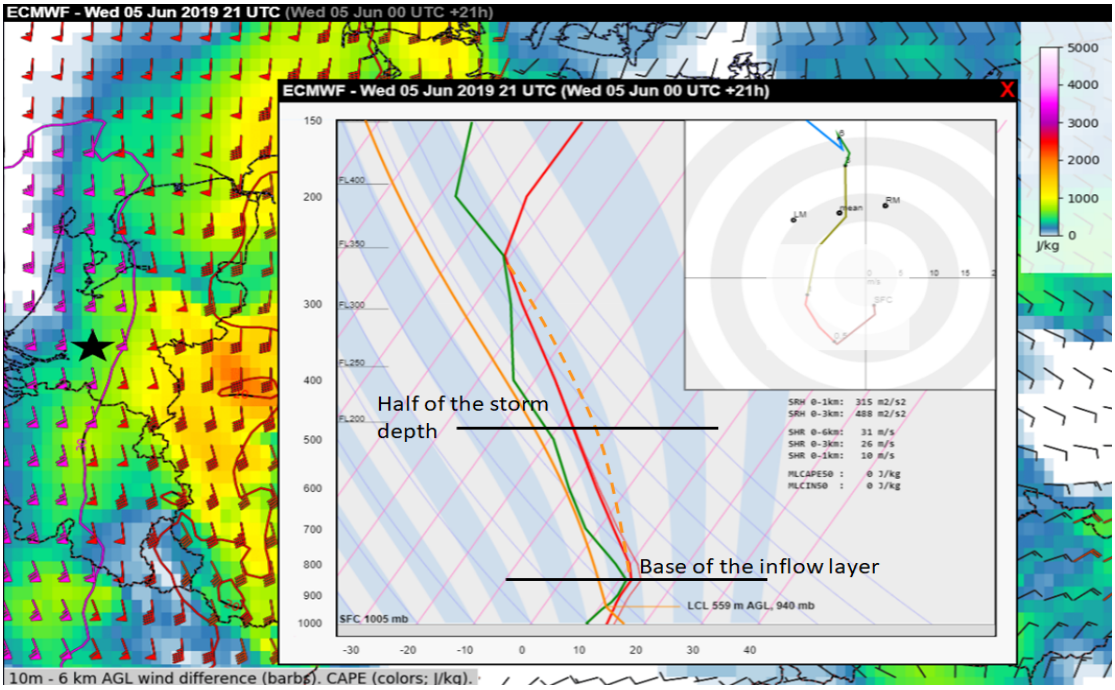

Figure 11. ECMWF 5 June 2019 00 UTC forecast of 21 UTC CAPE (shaded) and 0–6 km bulk vertical wind shear (barbs and contours). The forecast profile and hodograph are plotted for the location marked by a star. The inflow layer and half of the storm depth are indicated. The "ineffective" lower portion of the hodograph has been blurred.

4.2 Combinations of CAPE and bulk shear

The product and ratio of CAPE and bulk shear are sometimes used as diagnostic parameters. The ratio of CAPE and bulk shear is known as the **Bulk Richardson Number** (BRN) and was proposed by Moncrief and Green (1972) and adapted by Weisman and Klemp (1982) in their pioneering modelling study for anticipating the type of convective storm. It is a dimensionless number and is normally calculated as:

$$BRN = \frac{CAPE}{\frac{1}{2}\|\Delta\vec{u}\|^2}$$

where $\Delta\vec{u}$ is the difference between the 0–6 km mean wind and the 0–500 m mean wind. In the simulations of Weisman and Klemp (1982) supercells developed in environments with BRN values generally between 10 and 50, while less organised convection typically formed when BRN exceeded 50. In operational forecasting practice, the BRN is not used very often: the use of the wind shear magnitude (such as the 0–6 km bulk shear) to forecast convective type is often preferred over BRN. The type of organisation of convection is not very sensitive to the magnitude of CAPE, and almost exclusively depends on the denominator of the BRN, i.e. the shear.

Because storm severity depends both on the convective mode that can be anticipated by the magnitude of shear, and on CAPE which modulates it too, because higher CAPE promotes a higher convective

updraught intensity, the product of these two parameters CAPE and bulk shear, i.e. $CAPE \cdot \|\Delta\vec{u}\|^2$, is a good predictor of potential storm severity. Craven and Brooks (2004) demonstrated that it discriminated better between non-severe and severe thunderstorms than CAPE or bulk shear alone. Brooks et al. (2013), Púčik et al. (2015) and Taszarek et al. (2017) have shown that the relative frequency of severe convective storms increases strongly with increasing CAPE and bulk shear. The product of the square root of twice CAPE[1] and 0–6 km bulk shear, i.e. $\sqrt{2CAPE}$. $\|\Delta\vec{u}\|$, has been shown to discriminate well between non-severe and severe convective storms (Taszarek et al. 2017) using a threshold value of 400 m^2/s^2. Over the United States, most of the events with hail ≥ 5 cm, wind gusts ≥ 32+ m/s and F2 or stronger tornadoes were associated with the product of CAPE and 0–6 km bulk shear exceeding 20000 m^3/s^3 (Craven and Brooks 2004).

One of the first composite parameters developed was the **Energy-Helicity Index (EHI)**, calculated as the product of CAPE and storm-relative helicity in the 0–3 km layer divided by 160,000 (Davies 1993): Rasmussen and Blanchard (1998) and Thompson et al. (2003) found median values of 0.64 and 0.8, respectively, for non-tornadic supercells, and 1.5 and 2.1, respectively, for supercells with significant tornadoes. Across Europe, EHI values are lower because significant tornadoes typically occur with lower CAPE and SRH than across the Midwest of the United States. Taszarek et al. (2020) found that strong tornadoes (F2–F3) across Europe occur with a median value of 470 J/kg of MLCAPE, compared to 900 J/kg across the United States, whilst the median storm-relative helicity is 150 $m^2\ s^{-2}$ across Europe vs. 280 $m^2\ s^{-2}$ in the United States. Although higher values of EHI are more supportive of tornadoes in both regions, very high values of EHI are less frequent over Europe than over the U.S. Midwest. This means that the tornadoes in Europe in spite of these more modest EHI values – but with other factors apparently favourable enough to ensure their development – occur with lower values of EHI than over the U.S. Midwest.

Other parameters that have been developed based on the cases over the United States Midwest include the **Supercell Composite Parameter (SCP)** and the **Significant Tornado Parameter (STP)**. Both parameters were introduced by Thompson et al. (2003) and are calculated as a product of a number of factors. Each of these factors is a parameter that represents a favourable condition for supercells and tornadoes, respectively, and was subjectively calibrated to be 1 for a typical value found with a supercell or significant tornado.

SCP originally included CAPE, 0–6 km bulk shear and 0–3 km SRH in its calculation, and STP included CAPE, 0–6 km bulk shear, 0–1 km SRH and the Lifted condensation level (LCL). The formulations of the SCP and STP currently in use at NOAA's Storm Prediction Center include "*effective*" versions of these parameters:

$$SCP = \frac{MUCAPE}{1000\ Jkg^{-1}} \cdot \frac{ESRH}{50\ m^2s^{-2}} \cdot \frac{EBWD}{20\ ms^{-1}} \cdot \frac{-40\ Jkg^{-1}}{MUCIN}$$

[1] The factor 2 is not necessary for this statement to be true but is included because the theoretical maximum updraught speed resulting from the conversion of a given amount of CAPE to kinetic energy equals $\sqrt{2CAPE}$.

with these notes[2]

$$STP = \frac{MLCAPE}{1500\,Jkg^{-1}} \cdot \frac{ESSHR}{20\,ms^{-1}} \cdot \frac{ESRH}{150\,m^2s^{-2}} \cdot \frac{2000\,m - MLLCL}{1500\,m} \cdot \frac{200\,J\,kg + MLCIN}{150\,Jkg^{-1}}$$

with these notes[3].

Here, the "*effective"* versions of the parameters are used. MUCAPE is the most unstable CAPE of any parcel in the profile, ESRH is storm-relative helicity over the effective inflow layer, EBWD is the effective bulk shear. MLCAPE, MLLCL and MLCIN refer to the CAPE, Lifted Condensation Level and Convective Inhibition for a 100 hPa mixed-layer parcel. ESSHR equals EBWD, except that it always uses the wind at 10 m above ground level as the lower layer.

Kaltenböck et al. (2009) reported smaller values of SCP and STP associated with significant tornadoes over Europe compared to the values found by Thompson et al. (2003) over the United States. Probably, the reason is that CAPE, which in both SCP and STP is divided by a value of 1000 J/kg, is lower in European severe weather situations: 1000 J/kg is actually higher than the average CAPE observed with tornadoes over Europe (Groenemeijer and van Delden 2007; Púčik et al. 2015; Taszarek et al. 2017). Because of this, SCP and STP should only be used to highlight areas with the best collocation of ingredients and they should not be required to exceed any particular threshold for supercells or tornadoes to occur. And there are additional caveats in using these composite parameters; for instance, users should realize that a doubling of the SCP (STP) does not mean that the probability of a supercell (significant tornado) doubles as well (Doswell and Schultz 2006). Moreover, the risk of supercells or tornadoes occurring is still contingent on the formation of a convective storm within the potentially favourable environment that these parameters can identify, despite the inclusion of a CIN-based factor in the SCP and STP. Furthermore, composite parameters which include CAPE, such as the EHI, SCP or STP, have been shown to have a low forecasting skill in situations of high shear and low CAPE (Sherburn and Parker 2014). In such environments, CAPE is often rapidly built-up and then released by deep convection (Sherburn and Parker 2016; Gatzen 2020). Recognizing that advection of warm, moist air is of importance for this rapid creation of CAPE, Sherburn et al. (2016) created an empirical composite parameter (MOSH) that uses the 0–3 km lapse rate (LLLR) and advection of equivalent potential temperature θ_e (MAXTEVV) instead of CAPE. It also uses wind shear in the lowest 1.5 km instead of the more traditionally used 0–6 km bulk-shear:

[2] EBWD is divided by 20 m s^{-1} in the range of 10–20 m s^{-1}. EBWD less than 10 m s^{-1} is set to zero, and EBWD greater than 20 m s^{-1} is set to one. The MUCIN term is based on work by Gropp and Davenport (2018), August issue of Weather and Forecasting, and it is set to 1.0 when muCIN is greater than -40 kg^{-1}.

[3] The MLLCL term is set to 1.0 when MLLCL < 1000 m, and set to 0.0 when MLLCL > 2000 m; the MLCIN term is set to 1.0 when MLCIN > -50 J kg^{-1}, and set to 0.0 when MLCIN < -200; the EBWD term is capped at a value of 1.5 for EBWD > 30 m s^{-1}, and set to 0.0 when EBWD < 12.5 m s^{-1}. Lastly, the entire index is set to 0.0 when the effective inflow base is above the ground.

$$\mathrm{MOSH} = \frac{(\mathrm{LLLR} - 4\,\mathrm{K\,km^{-1}})^2}{4\,\mathrm{K^2\,km^{-2}}} \times \frac{(\mathrm{S15MG} - 8\,\mathrm{m\,s^{-1}})}{10\,\mathrm{m\,s^{-1}}} \times \frac{(\mathrm{MAXTEVV} + 10\,\mathrm{K\,Pa\,km^{-1}\,s^{-1}})}{9\,\mathrm{K\,Pa\,km^{-1}\,s^{-1}}}.$$

This parameter has been shown to have considerable skill in predicting severe wind and tornado events.

There are many other composite parameters that incorporate measures of vertical wind shear and were developed to address specific forecasting problems. Many of them are calculated as a forecasting guidance by the Storm Prediction Center in the United States. Such parameters include “large hail parameter”, which uses several metrics of wind shear, including the bulk shear between the ground and the Equilibrium level (Johnson and Sugden 2014). In addition, two such composite parameters were developed for forecasting wind-gust producing convective systems based on the works of Evans and Doswell (2001) and Cohen et al. (2007). Both parameters include measures of the mean wind and the deep-layer bulk shear.

Applying these composite indices and the associated threshold values stated in the literature may be problematic outside the regions for which they were originally developed. Many of the mentioned parameters have not been evaluated outside of the regions where they have been developed and this should be taken into consideration when using them in operational practice. Because of this, looking for the exceedance of a particular threshold is not recommended, but composite parameters can be used to identify where the best overlap of ingredients occurs.

5 Visualisations of vertical wind shear

Bulk shear is usually either plotted as the contours or wind barbs on a map. In some cases, barbs and contours are combined. Bulk-shear can be displayed together with CAPE, where CAPE is shaded, and bulk shear is displayed using wind barbs (Figure 12). Such a combination provides a quick diagnosis of where the most severe storms are possible in case they develop.

SRH, being a scalar quantity, cannot be plotted as vectors or wind barbs, so contours or shaded areas are typically used instead. A combination of a shaded SRH field and contours of CAPE is often used by ESSL, complemented with barbs representing storm motion calculated for a right-moving supercell (Figure 13).

Instead of shear vectors, wind vectors at different levels may be displayed, giving a crude idea about the length and shape of the hodograph (Figure 14). Wind barbs at different levels may be plotted as well, but in such a case it is more difficult to infer the hodograph shape (wind barbs are drawn in the direction from which blows, opposite to the wind vectors used to create the hodograph). Cameron J. Nixon has recently developed a visualization whereby miniature storm-relative hodographs are displayed directly. With each of these visualisations, plotting multiple vectors or barbs for each grid point can easily render the image too crowded. To mitigate this, the horizontal resolution of the displayed wind shear data has to be reduced, which can be problematic over areas with strong local variations.

The visualization platform used at ESSL for its courses and the ESSL Testbed (Groenemeijer et al, 2017), incorporates a roaming sounding feature, whereby soundings and wind shear profiles are interactively displayed when a user moves the mouse pointer across an NWP forecast map (Figure 15). This is rendered possible by bilinear interpolation of the NWP data to the location of the mouse pointer. The resulting quickly adjusting profile includes updated diagnostic parameters and mitigates the problem of the static maps in Figure 14, that features not resolved by the widely spaced vectors, barbs or hodographs, are invisible.

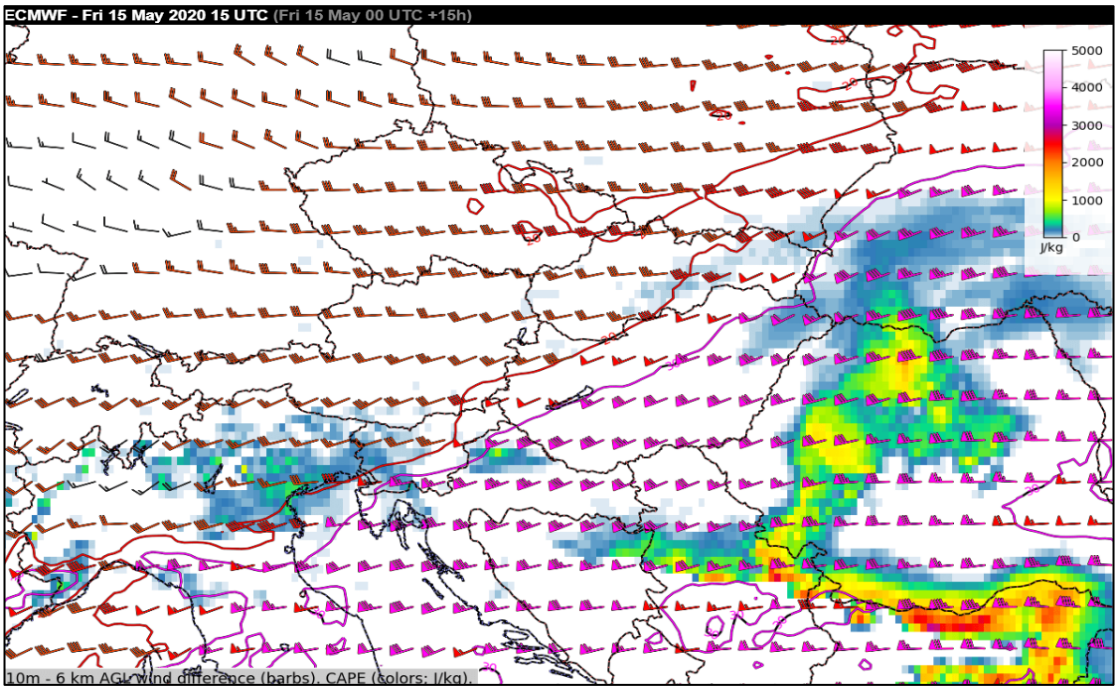

Figure 12. Visualisation of 0–6 km bulk shear (contours and wind-barbs) and CAPE (colour scale).

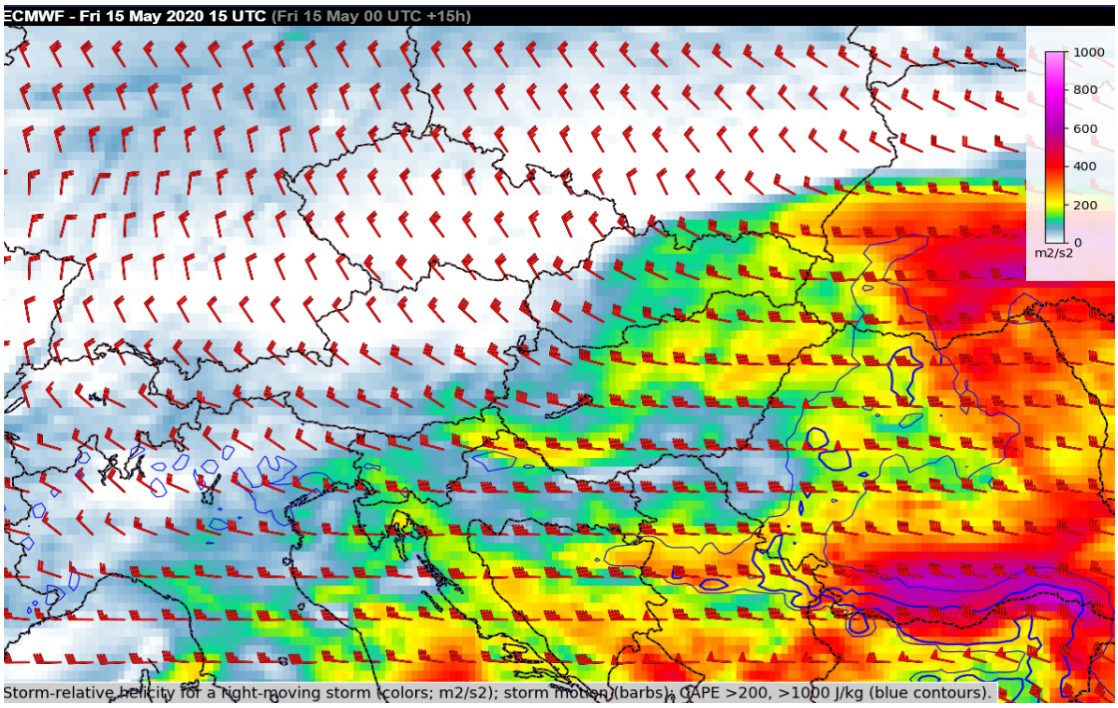

Figure 13. Visualisation of SRH (colour scale) along with CAPE (blue contours) and nominal motion of a right-moving supercell (wind barbs).

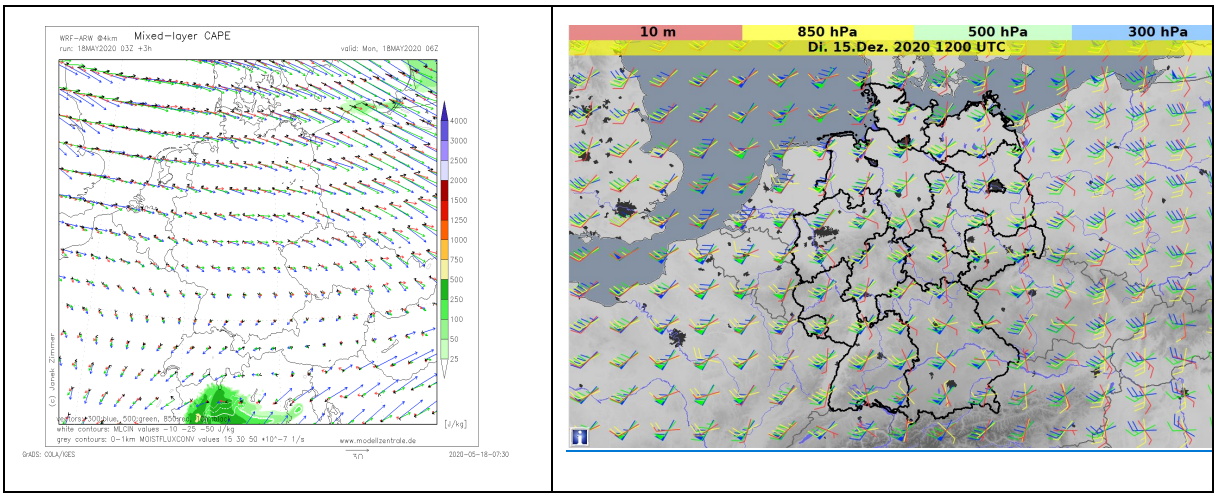

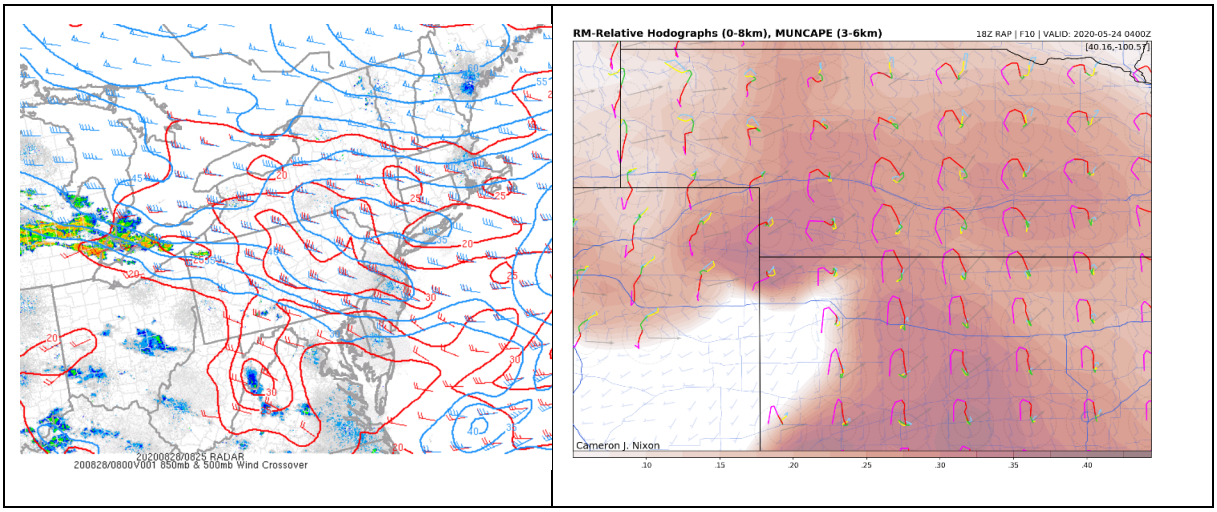

Figure 14. Visualisations of vertical wind shear using wind vectors at different altitudes plotted using arrows (left top, source: modellzentrale.de, courtesy: Janek Zimmer), wind barbs (right top, source: Deutscher Wetterdienst; left bottom, source: Storm Prediction Center), and miniature hodographs (right bottom, source: Cameron J. Nixon, cameronnixonphotography.wordpress.com).

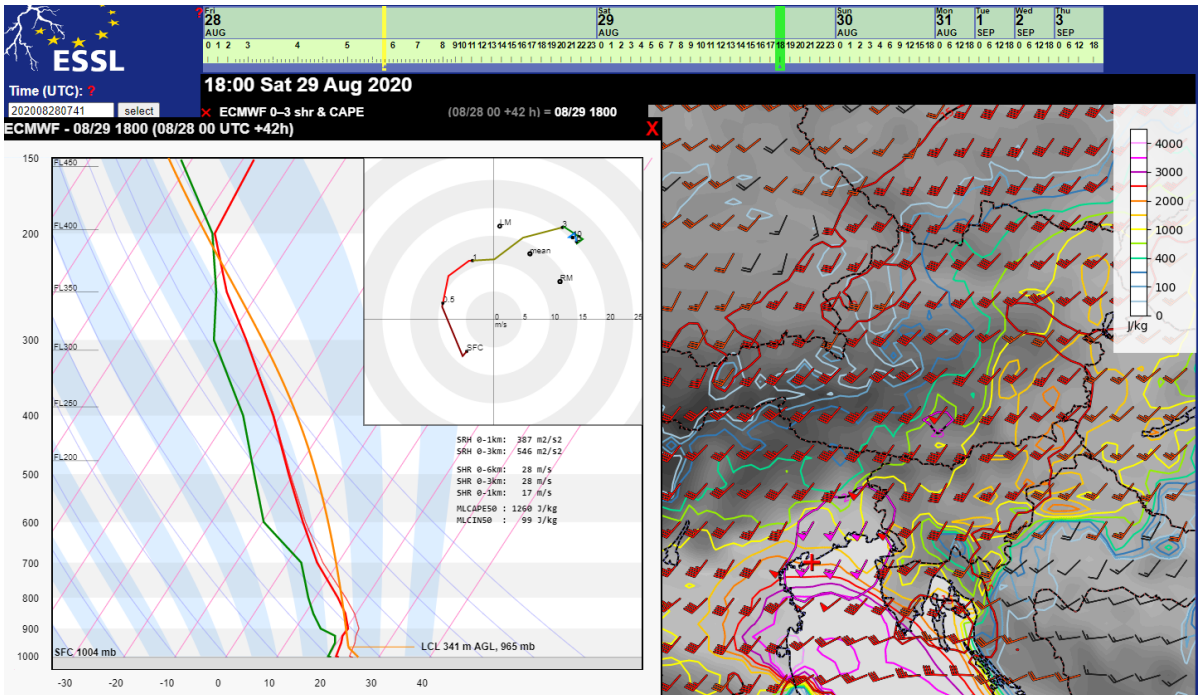

Figure 15. Interactive roaming sounding feature. The sounding, hodograph, and parameters adjust immediately when the red cross (here close to Venice, Italy) is moved across the map with the mouse pointer.

6 Wind shear parameters at ECMWF

Wind shear is an important ingredient for organisation of convection. Highly organised convection, such as supercells, tends to account for many of the major outbreaks of severe convective weather, as characterised by phenomena such as tornadoes, very large hail (5 cm diameter and over) and strong winds. Since 6th March 2016 ECMWF has been computing and providing operationally as a standard model output a **composite CAPE-shear parameter** "CAPES":

$$CAPES = WS_{925}^{500}\sqrt{CAPE},$$

where WS_{925}^{500} is the deep-layer bulk shear, approximated by the magnitude of the wind vector difference between 925 and 500-hPa pressure levels. It has been shown that the product of CAPE and deep-layer shear – a composite index – is a good discriminator between non-severe and severe thunderstorms (Craven and Brooks, 2004; Taszarek et al., 2017). CAPES is a parameter to which ECMWF's ensemble-based Extreme Forecast Index (EFI) and Shift Of Tails index (SOT) concepts have been applied, and the resulting fields have been shown to have significant skill in forecasting severe convective outbreaks in the medium range (Tsonevsky et al., 2018; Tsonevsky, 2015).

An outbreak of severe convection affected northern Italy on 29 August 2020 (Figure 16). On that day a trough was approaching Italy from the west and the southwesterly flow in the mid troposphere was strengthening over the northern part of the country. Deep-layer 0-6 km shear peaked at around 25 ms^{-1} in the presence of unstable air, with CAPE over 1500 Jkg^{-1}. The composite CAPE-shear index was extreme compared to the model climatology, resulting in high values of the EFI for this parameter being computed from the ECMWF ensemble system in the medium range (Figure 16b). Positive SOT in the area indicated that the top 10% of the ensemble forecasts for CAPE-shear exceeded the 99th percentile of the model climate. A number of reports of large hail, strong winds and an F1 tornado were recorded in the European Severe Weather Database (ESWD; Figure 16a).

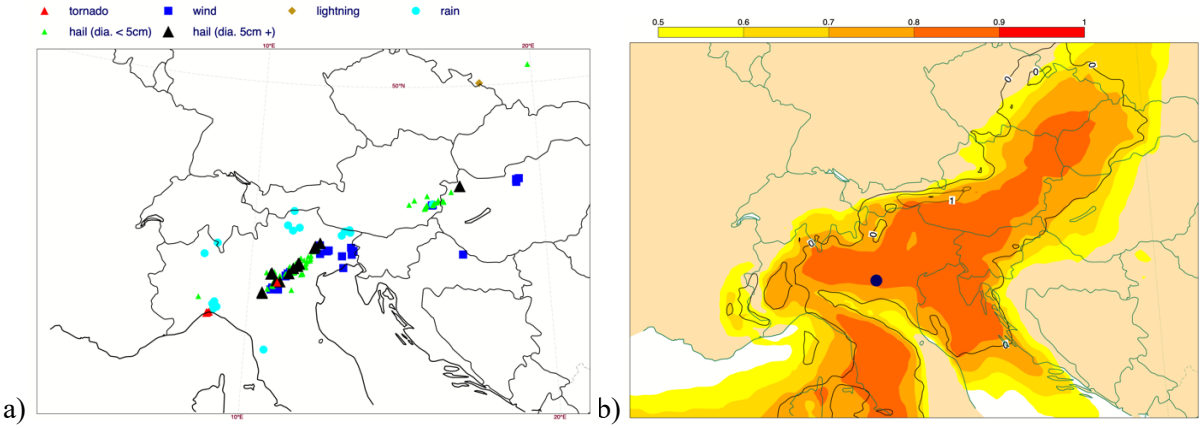

Figure 16. Severe convective outbreak over northern Italy on 29 August 2020 a) Severe weather reports from ESWD. Symbols denote different types of convective hazards as shown in the legend. Hail reports with hail stone diameter of at least 2 cm but less than 5 cm are marked with green triangles, and for diameters of 5 cm and over – with black triangles; b) T+96-120h EFI/SOT forecast for CAPE-shear valid for 29 August 2020. Values of the EFI > 0.5 are shaded. Black contours denote SOT=0,1,2. Navy circle marks the location where the forecast in Figure 19 is valid.

For the computation of the CAPE-shear EFI the maximum value in 24-hours is retained from a newly implemented parameter maximum CAPE-shear in the last 6 hours (ShortName=mxcapes6 in the GRIB parameter database) which represents the maximum CAPE-shear computed using hourly model output. Figure 17 shows the maximum CAPE-shear in 24 hours, computed from mxcapes6, for the ECMWF high-resolution forecast. In the area of severe convective weather over Italy in Figure 16a CAPE-shear values in the forecast are around the 99th percentile of the Model climate used for the computation of the EFI. The parameter mxcape6 for the high-resolution forecast as well as a set of Model climate percentiles are available on ECMWF's forecaster-oriented web service ecCharts.

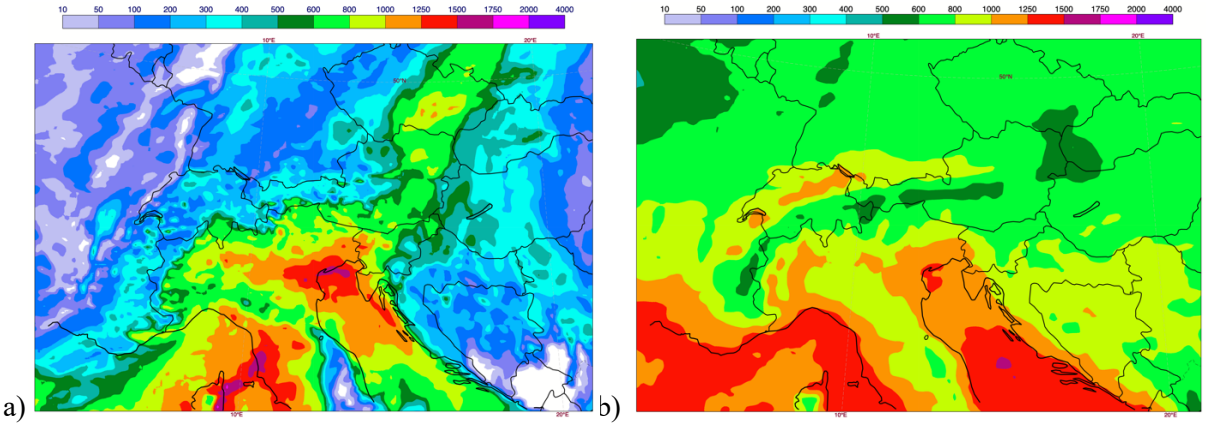

Figure 17. Maximum CAPE-shear (in m^2s^{-2}) computed from mxcapes6 for the same 24-hour period as on Figure 16, commencing 00 UTC on 29 August 2020 for a) T+96-120h ECMWF high-resolution forecast and b) 99th percentile of the Model climate computed from ECMWF re-forecasts and used for the computation of the EFI.

The **wind hodograph** is another wind-shear-related representation provided by ECMWF as a part of the ensemble vertical profile product (Figure 18) since 5 June 2018. It displays winds at different pressure levels (1000, 925, 850, 700, 600, 500, 400, 300, 250, 200 and 100 hPa). Each line represents forecasts from an ensemble member (50 in total), or ECMWF's high-resolution run (HRES, very thick) or the Control run (thick), whilst colours denote different layers in the atmosphere. Such wind hodographs provide a visualisation of wind shear in different layers as well as indicating whether it is chiefly directional or speed shear.

For forecasting deep moist convection, wind hodographs can be used along with the accompanying CAPE/CIN diagram (Figure 18) which represents the distribution of Convective Available Potential Energy (CAPE) for three different bins of Convective Inhibition (CIN).

Figure 19 shows T+108h forecast wind hodographs and a CAPE/CIN diagram for a location over northern Italy affected by severe convection on 29 August 2020 (as in Figure 16). The forecast valid for 12 UTC on 29 August gives moderate instability (CAPE~1000 Jkg^{-1}) and long curved wind hodographs, especially in the atmospheric layer between 1000 and 700 hPa, which are capable of supporting supercell development. Very large hail up to 8 cm diameter and strong wind gusts were reported in that area (Figure 16a).

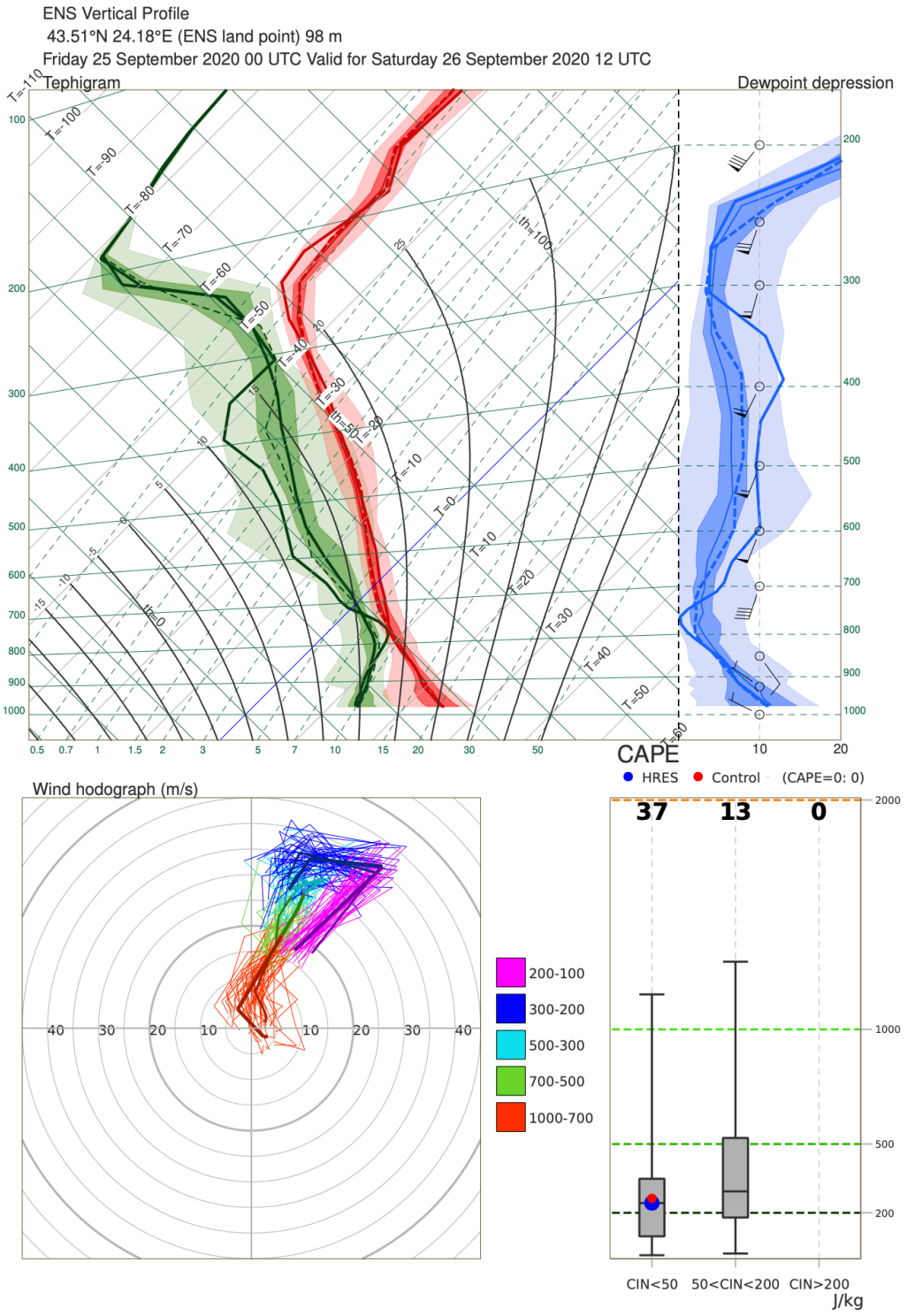

Figure 18. Vertical profile product based on ECMWF forecasts includes wind hodographs. On the wind hodograph plot the thick line represents HRES and the thinner one – the Control forecast.

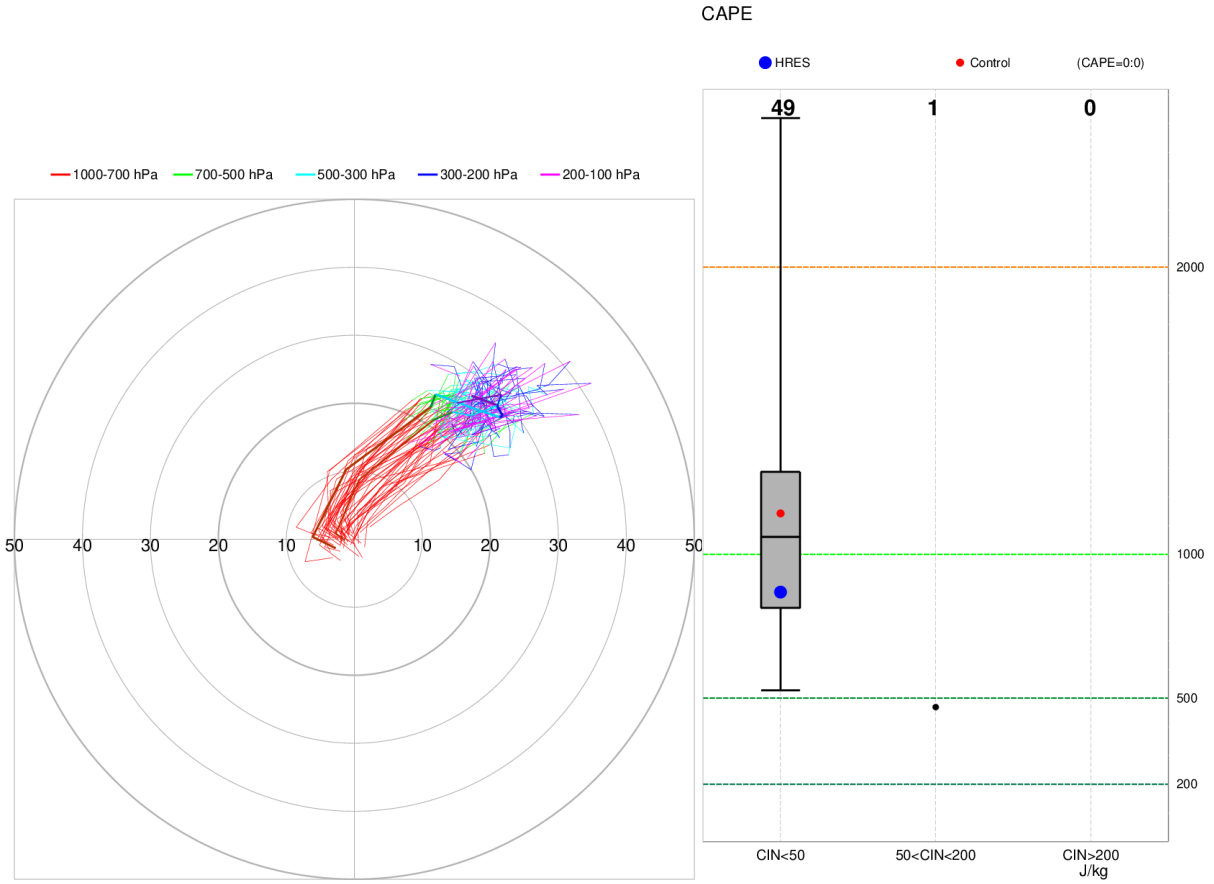

Figure 19. Wind hodographs and CAPE/CIN diagram for a location in northern Italy with geographical coordinates 45.6N/11.5E affected by severe thunderstorms on 29 August 2020. The T+108h forecast is initialised at 00 UTC on 25 August 2020 valid for 12 UTC on 29 August 2020. Numbers on CAPE/CIN plot represent the ensemble population of each bin. Same case and data time as shown on Figure 16.

Together with the pre-computed 925-500 hPa bulk shear used for the computation of the CAPE-shear EFI and SOT, users can also display bulk shear for other layer combinations of their choice, for HRES, using ECMWF's web chart service ecCharts. Such fields can be combined with other forecast fields, such as CAPE and 500 hPa geopotential, as an additional tool for forecasting deep, moist convection (Figure 20). Ample levels are currently available for selection in ecCharts, providing great flexibility for users – namely the 10 m and 100 m-above-ground level and pressure levels of 925, 850, 800, 700, 600, 500, 300, 250 and 200 hPa. The product example shown in Figure 20 can help identifying where CAPE and high deep-layer shear co-exist, and so may sustain severe thunderstorms, whilst the geopotential forecast puts this into a synoptic-scale context. ECMWF has recently added deep-layer 10m–500hPa (0–6 km) shear as a vector field on ecCharts (Figure 20b) so that direction can also be visualised. The direction of the vertical shear vector can be used to infer where new cell formation will take place in multicell situations. According to the RKW theory (Rotunno et al. 1988), the deepest lift can be found on the downshear flank of the gust front (e.g. on the eastern flank of the storm if westerly shear is present in the environment). For this purpose, one should use the shear vector from a layer that approximates the depth of a typical cold pool which can vary from few hundred metres to several

kilometres. In some cases, linearly organised mutlicells (squall lines / bow-echoes) will move faster than predicted by the mean wind. Such behaviour occurs if shear vectors point in the same direction as the mean wind, so that thunderstorms the movement caused by the formation of new cells (downshear) adds to the movement due to the advection of individual cells by the mean wind. Dial et al. (2010) investigated the relationship between convective mode evolution (discrete storms vs linear systems) and the orientation of vertical shear vectors with respect to the initiating synoptic boundary (e.g. cold fronts). They found that thunderstorms which were initially mostly discrete tended to evolve into linear systems when the component of the deep-layer shear vectors that was normal to the initiating boundary was small. Conversely when this was large storms tended to remain discrete.

a)

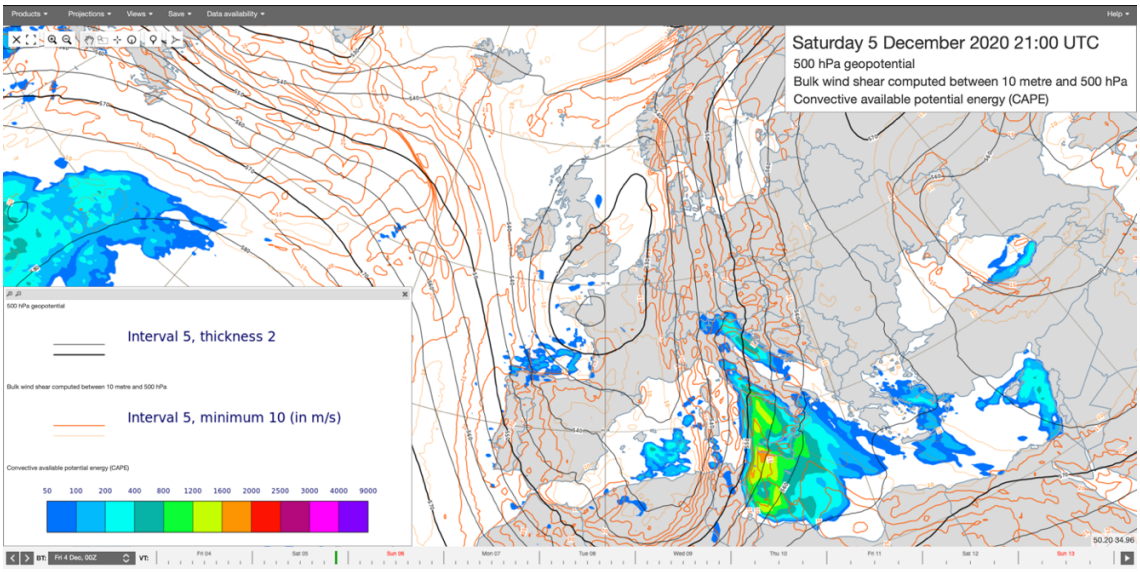

b)

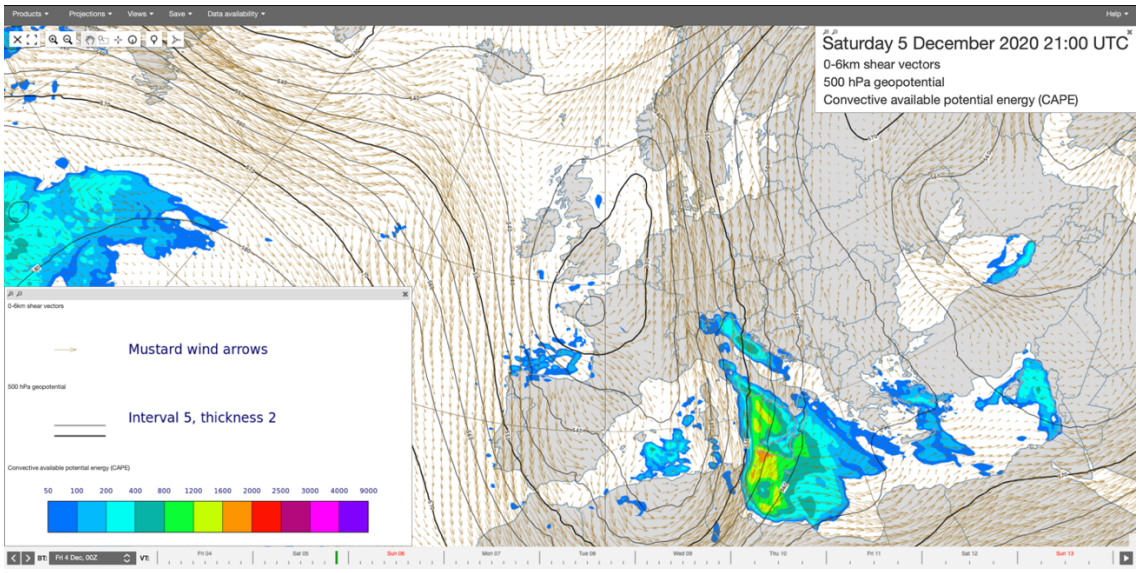

Figure 20. a) HRES 10m–500 hPa bulk shear (contours), 500-hPa geopotential (black contours) and CAPE (shaded); b) HRES 10m-500 hPa bulk shear plotted as vectors, 500-hPa geopotential (black contours) and CAPE (shaded). The user can also activate a movable cursor so that precise values of the 3 variables can be read off for any site.

SRH has been recognized as an important parameter in forecasting rotation in severe thunderstorms. ECMWF is considering computing SRH from the IFS data; to respond to requests received from ECMWF's member states and the wider meteorological community.

In addition, from the forecaster's perspective, storm motion can be an important parameter depending on the convective storm type. With increasing the model resolution, storm motion is becoming an even more valuable diagnostic from the IFS, potentially opening the door to improvements in forecasting of high impact weather events such as torrential rain and flash floods.

7 Ongoing research

Recently, statistical relationships have been developed that quantify the probability of convective hazards as a function of parameters characterizing a storm's environment, such as CAPE and measures of wind shear (Togstad et al, 2011; Hart and Cohen 2016; Rädler et al. 2018). Such models combine multiple variables and confirm the strong link between severe convective storms and wind shear. Environmental parameters (e.g. deep-layer shear) have been compared to the characteristics of explicitly simulated cells in convection-allowing models (Gagne et al. 2019; Burke et al. 2020). Statistical models or machine-learning approaches provide an objective forecast of severe weather likelihood that would otherwise result from a subjective assessment by forecasters. First studies show that such objective forecasts can provide forecasts that are on a par with subjective forecasts or can even surpass their quality, at least at for lead times of more than 24 hours (Burke et al. 2020; Hill et al. 2020).

Besides using environmental parameters from a point-wise perspective, spatial patterns of parameters have become a topic of current research too, e.g. using self-organizing maps (Anderson-Frey et al. 2017; Anderson-Frey and Brooks 2019), or composites (Kunz et al, 2020). These studies show that severe weather typically occurs along the edge of, rather than deep within, the areas with seemingly the best environmental conditions for severe storms.

Much work is being done on using idealised numerical simulations to study the effects of vertical wind shear on convective storms, their updraughts (Marion and Trapp 2019; Peters et al. 2019a and b), tornadogenesis (Orf et al. 2017; Coffer and Parker 2018) or hail growth (Dennis and Kumjian 2017). Such research involves also formulation of new parameters that may help with forecasting of severe convection (Alfaro and Coniglio 2018; Coffer et al. 2019).

Explicit simulation with convection-allowing models enables investigation of the predictability of convection in different regimes of vertical wind shear. One of the first studies of this topic found that the intensity of storms in weak shear is less predictable than those that develop in strong shear. Another finding is that small changes in buoyancy can determine whether a storm survives in the strongly sheared environments (Lawson, 2019). These results hint at explanations for why forecasts and warnings for severe convective storms tend to be less skilful in regimes of low CAPE and high shear, and in regimes of weak vertical wind shear, regardless of CAPE (Anderson-Frey et al. 2016; Herman et al. 2018).

References

Alfaro, D.A., 2017. Low-tropospheric shear in the structure of squall lines: Impacts on latent heating under layer-lifting ascent. *Journal of the Atmospheric Sciences*, **74**, 229–248. https://doi.org/10.1175/JAS-D-16-0168.1

Alfaro, D.A. and Coniglio, M.C., 2018. Discrimination of mature and dissipating severe-wind-producing MCSs with layer-lifting indices. *Weather and Forecasting*, **33**, 3–21. https://doi.org/10.1175/WAF-D-17-0088.1

Allen, J.T. and Karoly, D.J., 2014. A climatology of Australian severe thunderstorm environments 1979–2011: inter-annual variability and ENSO influence. *International Journal of Climatology*, **34**, 81–97. https://doi.org/10.1002/joc.3667

Anderson-Frey, A.K., Richardson, Y.P., Dean, A.R., Thompson, R.L. and Smith, B.T., 2016. Investigation of near-storm environments for tornado events and warnings. *Weather and Forecasting*, **31**, 1771–1790. https://doi.org/10.1175/WAF-D-16-0046.1

Anderson-Frey, A.K., Richardson, Y.P., Dean, A.R., Thompson, R.L. and Smith, B.T., 2017. Self-organizing maps for the investigation of tornadic near-storm environments. *Weather and Forecasting*, **32**, 1467–1475. https://doi.org/10.1175/WAF-D-17-0034.1

Anderson-Frey, A.K. and Brooks, H., 2019. Tornado Fatalities: An Environmental Perspective. *Weather and Forecasting*, **34**, 1999–2015. https://doi.org/10.1175/WAF-D-19-0119.1

Antonescu, B., D. M. Schultz, F. Lomas, and T. Kühne, 2016: Tornadoes in Europe: Synthesis of the Observational Datasets. *Monthly Weather Review*, **144**, 2445–2480. https://doi.org/10.1175/MWR-D-15-0298.1

Berthet, C., Wesolek, E., Dessens, J. and Sanchez, J.L., 2013. Extreme hail day climatology in Southwestern France. *Atmospheric Research*, **123**, 139–150. https://doi.org/10.1016/j.atmosres.2012.10.007

Blair, S.F., Laflin, J.M., Cavanaugh, D.E., Sanders, K.J., Currens, S.R., Pullin, J.I., Cooper, D.T., Deroche, D.R., Leighton, J.W., Fritchie, R.V. and Mezeul II, M.J., 2017. High-resolution hail observations: Implications for NWS warning operations. *Weather and Forecasting*, **32**, 1101–1119. https://doi.org/10.1175/WAF-D-16-0203.1

Brady, R. H., and E. J. Szoke, 1989: A case study of non-mesocyclone tornado development in northeast Colorado: Similarities to waterspout formation. *Monthly Weather Review*, **117**, 843–856. https://doi.org/10.1175/1520-0493(1989)117%3C0843:ACSONT%3E2.0.CO;2

Bryan, G.H., Knievel, J.C. and Parker, M.D., 2006. A multimodel assessment of RKW theory's relevance to squall-line characteristics. *Monthly Weather Review*, **134**, 2772–2792. https://doi.org/10.1175/MWR3226.1

Brooks, H.E. and Doswell III, C.A., 1993. Extreme winds in high-precipitation supercells. In *Preprints, 17th Conf. on Severe Local Storms, St. Louis, MO, Amer. Meteor. Soc*, 173–177. https://pdfs.semanticscholar.org/324c/a3ffce3408c6cb49d35ade7347ddf24b56f1.pdf

Brooks, H.E., Doswell III, C.A. and Wilhelmson, R.B., 1994. The role of midtropospheric winds in the evolution and maintenance of low-level mesocyclones. *Monthly Weather Review*, **122**, 126–136. https://doi.org/10.1175/1520-0493(1994)122%3C0126:TROMWI%3E2.0.CO;2

Brooks, H.E., 2009. Proximity soundings for severe convection for Europe and the United States from reanalysis data. *Atmospheric Research*, **93**, 546–553. https://doi.org/10.1016/j.atmosres.2008.10.005

Brooks, H.E., 2013. Severe thunderstorms and climate change. *Atmospheric Research*, **123**, 129–138. https://doi.org/10.1016/j.atmosres.2012.04.002

Browning, K.A., 1964. Airflow and precipitation trajectories within severe local storms which travel to the right of the winds. *Journal of the Atmospheric Sciences*, **21**, 634–639. https://doi.org/10.1175/1520-0469(1964)021%3C0634:AAPTWS%3E2.0.CO;2

Bunkers, M.J., Klimowski, B.A., Zeitler, J.W., Thompson, R.L. and Weisman, M.L., 2000. Predicting supercell motion using a new hodograph technique. *Weather and Forecasting*, **15**, 61-79. https://doi.org/10.1175/1520-0434(2000)015%3C0061:PSMUAN%3E2.0.CO;2

Bunkers, M.J., Johnson, J.S., Czepyha, L.J., Grzywacz, J.M., Klimowski, B.A. and Hjelmfelt, M.R., 2006. An observational examination of long-lived supercells. Part II: Environmental conditions and forecasting. *Weather and forecasting*, **21**, pp.689-714 https://doi.org/10.1175/WAF952.1

Bunkers, M.J., 2018. Observations of right-moving supercell motion forecast errors. *Weather and Forecasting*, **33**, 145–159. https://doi.org/10.1175/WAF-D-17-0133.1

Burke, A., Snook, N., Gagne II, D.J., McCorkle, S. and McGovern, A., 2020. Calibration of Machine Learning–Based Probabilistic Hail Predictions for Operational Forecasting. *Weather and Forecasting*, **35**, 149–168. https://doi.org/10.1175/WAF-D-19-0105.1

Chisholm, A. J., and J. H. Renick, 1972: The kinematics of multi-cell and supercell Alberta hailstorms. Research Council of Alberta Hail Studies Report **72-2**, 24–31.

Coffer, B.E. and Parker, M.D., 2017. Simulated supercells in nontornadic and tornadic VORTEX2 environments. *Monthly Weather Review*, **145**, 149–180. https://doi.org/10.1175/MWR-D-16-0226.1

Coffer, B.E. and Parker, M.D., 2018. Is there a “tipping point” between simulated nontornadic and tornadic supercells in VORTEX2 environments?. *Monthly Weather Review*, **146**, 2667–2693. https://doi.org/10.1175/MWR-D-18-0050.1

Coffer, B.E., Parker, M.D., Thompson, R.L., Smith, B.T. and Jewell, R.E., 2019. Using near-ground storm-relative helicity in supercell tornado forecasting. *Weather and Forecasting*, **34**, 1417–1435. https://doi.org/10.1175/WAF-D-19-0115.1

Cohen, A.E., Coniglio, M.C., Corfidi, S.F. and Corfidi, S.J., 2007. Discrimination of mesoscale convective system environments using sounding observations. *Weather and Forecasting*, **22**, 1045–1062. https://doi.org/10.1175/WAF1040.1

Coniglio, M.C., Stensrud, D.J. and Wicker, L.J., 2006. Effects of upper-level shear on the structure and maintenance of strong quasi-linear mesoscale convective systems. *Journal of the Atmospheric Sciences*, **63**, 1231–1252. https://doi.org/10.1175/JAS3681.1

Corfidi, S.F., Meritt, J.H. and Fritsch, J.M., 1996. Predicting the movement of mesoscale convective complexes. *Weather and Forecasting*, **11**, 41–46. https://doi.org/10.1175/1520-0434(1996)011%3C0041:PTMOMC%3E2.0.CO;2

Corfidi, S.F., 2003. Cold pools and MCS propagation: Forecasting the motion of downwind-developing MCSs. *Weather and Forecasting*, **18**, 997–1017. https://doi.org/10.1175/1520-0434(2003)018%3C0997:CPAMPF%3E2.0.CO;2

Craven, J.P. and Brooks, H.E, 2004. Baseline climatology of sounding derived parameters associated with deep, moist convection. *National Weather Digest*, **28**, 13–24. https://www.nssl.noaa.gov/users/brooks/public_html/papers/cravenbrooksnwa.pdf

Davies, J.M., 1993. Hourly helicity, instability, and EHI in forecasting supercell tornadoes. In *Preprints, 17th Conf. on Severe Local Storms, St. Louis, MO, 1993*, 107–111.

Davies, J.M., 2006. Tornadoes in environments with small helicity and/or high LCL heights. *Weather and Forecasting*, **21**, 579–594. https://doi.org/10.1175/WAF928.1

Davies-Jones, R., 1984. Streamwise vorticity: The origin of updraft rotation in supercell storms. *Journal of the Atmospheric Sciences*, **41**, 2991–3006. https://doi.org/10.1175/1520-0469(1984)041%3C2991:SVTOOU%3E2.0.CO;2

Davies-Jones, R.P., D.W. Burgess and M. Foster, 1990: Test of helicity as a tornado forecast parameter. *Preprints*, *16th Conf. on Severe Local Storms, Kananaskis Park, AB, Canada, Amer. Meteor. Soc.*, 588-592.

Dennis, E.J. and Kumjian, M.R., 2017. The impact of vertical wind shear on hail growth in simulated supercells. *Journal of the Atmospheric Sciences*, **74**, 641–663. https://doi.org/10.1175/JAS-D-16-0066.1

Dial, G.L., Racy, J.P. and Thompson, R.L., 2010. Short-term convective mode evolution along synoptic boundaries. *Weather and Forecasting*, **25**, 1430–1446. https://doi.org/10.1175/2010WAF2222315.1

Doswell, C. A., III, H. E. Brooks, and R. A. Maddox, 1996: Flash flood forecasting: An ingredients-based methodology. *Weather and Forecasting*, **11**, 560–581. https://doi.org/10.1175/1520-0434(1996)011%3C0560:FFFAIB%3E2.0.CO;2

Doswell III, C.A. and Evans, J.S., 2003. Proximity sounding analysis for derechos and supercells: An assessment of similarities and differences. *Atmospheric Research*, **67**, 117–133. https://doi.org/10.1016/S0169-8095(03)00047-4

Doswell III, C.A. and Schultz, D.M., 2006. On the use of indices and parameters in forecasting severe storms. *E-Journal of Severe Storms Meteorology*, **1**, 3. https://www.ejssm.org/ojs/index.php/ejssm/article/viewArticle/11/12

Edwards, R. and Thompson, R.L., 1998. Nationwide comparisons of hail size with WSR-88D vertically integrated liquid water and derived thermodynamic sounding data. *Weather and Forecasting*, **13**, 277–285. https://doi.org/10.1175/1520-0434(1998)013%3C0277:NCOHSW%3E2.0.CO;2

Evans, J.S. and Doswell III, C.A., 2001. Examination of derecho environments using proximity soundings. *Weather and Forecasting*, **16**, 329–342. https://doi.org/10.1175/1520-0434(2001)016%3C0329:EODEUP%3E2.0.CO;2

Fankhauser, J. C., 1988: Estimates of Thunderstorm Precipitation Efficiency from Field Measurements in CCOPE. *Monthly Weather Review*, **116**, 663–684. https://doi.org/10.1175/1520-0493(1988)116%3C0663:EOTPEF%3E2.0.CO;2

Gagne II, D.J., Haupt, S.E., Nychka, D.W. and Thompson, G., 2019. Interpretable deep learning for spatial analysis of severe hailstorms. *Monthly Weather Review*, **147**, 2827–2845. https://doi.org/10.1175/MWR-D-18-0316.1

Gatzen, C., 2013. Warm-season severe wind events in Germany. *Atmospheric Research*, **123**, 197–205. https://doi.org/10.1016/j.atmosres.2012.07.017

Gatzen, C.P., Fink, A.H., Schultz, D.M. and Pinto, J.G., 2020. An 18-year climatology of derechos in Germany. *Natural Hazards and Earth System Sciences*, **20**, pp.1335-1335. https://doi.org/10.5194/nhess-20-1335-2020

Grams, J.S., Thompson, R.L., Snively, D.V., Prentice, J.A., Hodges, G.M. and Reames, L.J., 2012. A climatology and comparison of parameters for significant tornado events in the United States. *Weather and Forecasting*, **27**, 106–123. https://doi.org/10.1175/WAF-D-11-00008.1

Groenemeijer, P.H. and Van Delden, A., 2007. Sounding-derived parameters associated with large hail and tornadoes in the Netherlands. *Atmospheric Research*, **83**, 473–487. https://doi.org/10.1016/j.atmosres.2005.08.006

Groenemeijer, P., and co-authors, 2017: Severe Convective Storms in Europe: Ten Years of Research and Education at the European Severe Storms Laboratory. *Bull. Amer. Meteor. Soc.*, **98**, 2641–2651. https://doi.org/10.1175/BAMS-D-16-0067.1

Hart, J.A. and Cohen, A.E., 2016. The statistical severe convective risk assessment model. *Weather and Forecasting*, **31**, 1697–1714. https://doi.org/10.1175/WAF-D-16-0004.1

Herman, G.R., Nielsen, E.R. and Schumacher, R.S., 2018. Probabilistic verification of Storm Prediction Center convective outlooks. *Weather and Forecasting*, **33**, 161–184. https://doi.org/10.1175/WAF-D-17-0104.1

Hill, A. J., G. R. Herman, and R. S. Schumacher, 2020: Forecasting Severe Weather with Random Forests. *Monthly Weather Review*, **148**, 2135–2161. https://doi.org/10.1175/MWR-D-19-0344.1

Hitchens, N.M. and Brooks, H.E., 2013. Preliminary investigation of the contribution of supercell thunderstorms to the climatology of heavy and extreme precipitation in the United States. *Atmospheric Research*, **123**, 206–210. https://doi.org/10.1016/j.atmosres.2012.06.023

Houston, A.L., Thompson, R.L. and Edwards, R., 2008. The optimal bulk wind differential depth and the utility of the upper-tropospheric storm-relative flow for forecasting supercells. *Weather and Forecasting*, **23**, 825–837. https://doi.org/10.1175/2008WAF2007007.1

Johns, R. H., and C. A. Doswell III, 1992: Severe local storms forecasting. *Weather and Forecasting*, **7**, 588–612. https://doi.org/10.1175/1520-0434(1992)007<0588:SLSF>2.0.CO;2

Johnson, A.W. and Sugden, K.E., 2014. Evaluation of sounding-derived thermodynamic and wind-related parameters associated with large hail events. *E-Journal of Severe Storms Meteorology*, **9**, 5. https://ejssm.org/ojs/index.php/ejssm/article/viewArticle/137

Kerr, B.W. and Darkow, G.L., 1996. Storm-relative winds and helicity in the tornadic thunderstorm environment. *Weather and Forecasting*, **11**, 489–505. https://doi.org/10.1175/1520-0434(1996)011%3C0489:SRWAHI%3E2.0.CO;2

Kirkpatrick, C., McCaul Jr, E.W. and Cohen, C., 2009. Variability of updraft and downdraft characteristics in a large parameter space study of convective storms. *Monthly weather review*, **137,** 1550–1561. https://doi.org/10.1175/2008MWR2703.1

Klemp, J.B. and Wilhelmson, R.B., 1978. The simulation of three-dimensional convective storm dynamics. *Journal of the Atmospheric Sciences*, **35**, 1070–1096. https://doi.org/10.1175/1520-0469(1978)035%3C1070:TSOTDC%3E2.0.CO;2

Kuchera, E.L. and Parker, M.D., 2006. Severe convective wind environments. *Weather and Forecasting*, **21**, 595–612. https://doi.org/10.1175/WAF931.1

Kunz, M., Wandel, J., Fluck, E., Baumstark, S., Mohr, S., and Schemm, S.: Ambient conditions prevailing during hail events in central Europe, *Natural Hazards and Earth System Sciences*, **20**, 1867–1887. https://doi.org/10.5194/nhess-20-1867-2020

Lawson, J.R., 2019. Predictability of Idealized Thunderstorms in Buoyancy–Shear Space. *Journal of the Atmospheric Sciences*, *76*(9), pp.2653-2672. https://doi.org/10.1175/JAS-D-18-0218.1

Maddox, R.A., 1976. An evaluation of tornado proximity wind and stability data. *Monthly Weather Review*, **104**, 133–142. https://doi.org/10.1175/1520-0493(1976)104%3C0133:AEOTPW%3E2.0.CO;2

Manzato, A., 2012. Hail in northeast Italy: Climatology and bivariate analysis with the sounding-derived indices. *Journal of Applied Meteorology and Climatology*, **51**, 449–467. https://doi.org/10.1175/JAMC-D-10-05012.1

Marion, G.R. and Trapp, R.J., 2019. The dynamical coupling of convective updrafts, downdrafts, and cold pools in simulated supercell thunderstorms. *Journal of Geophysical Research: Atmospheres*, **124**, 664–683. https://doi.org/10.1029/2018JD029055

Markowski, P. and Richardson, Y., 2010. *Mesoscale Meteorology in Midlatitudes*. John Wiley & Sons. https://doi.org/10.1002/9780470682104

Markowski, P.M. and Richardson, Y.P., 2014. The influence of environmental low-level shear and cold pools on tornadogenesis: Insights from idealized simulations. *Journal of the Atmospheric Sciences*, **71**, 243–275. https://doi.org/10.1175/JAS-D-13-0159.1

Marwitz, J. D., 1972a: Precipitation efficiency of thunderstorms on the high plains. *J. Res. Atmos.*, **6**, 367–370.

McCaul Jr, E. W., & Weisman, M. L. (2001). The sensitivity of simulated supercell structure and intensity to variations in the shapes of environmental buoyancy and shear profiles. *Monthly Weather Review*, **129**, 664–687. https://doi.org/10.1175/1520-0493(2001)129%3C0664:TSOSSS%3E2.0.CO;2

Moncrieff, M.W. and Green, J.S.A., 1972. The propagation and transfer properties of steady convective overturning in shear. *Quarterly Journal of the Royal Meteorological Society*, **98**, pp.336-352. https://doi.org/10.1002/qj.49709841607

Nelson, S.P., 1987. The hybrid multicellular–supercellular storm—An efficient hail producer. Part II. General characteristics and implications for hail growth. *Journal of the Atmospheric Sciences*, **44**, 2060–2073. https://doi.org/10.1175/1520-0469(1987)044%3C2060:THMSEH%3E2.0.CO;2

Newton, C.W., 1960. Morphology of thunderstorms and hailstorms as affected by vertical wind shear. *Physics of Precipitation, Geophysical Monographs*, **5**, 339–347. https://doi.org/10.1029/GM005p0339

Nielsen, E.R. and Schumacher, R.S., 2018. Dynamical insights into extreme short-term precipitation associated with supercells and mesovortices. *Journal of the Atmospheric Sciences*, **75**, 2983–3009. https://doi.org/10.1175/JAS-D-17-0385.1

Nowotarski, C.J. and Jensen, A.A., 2013. Classifying proximity soundings with self-organizing maps toward improving supercell and tornado forecasting. *Weather and Forecasting*, **28**, 783–801. https://doi.org/10.1175/WAF-D-12-00125.1

Orf, L., Wilhelmson, R., Lee, B., Finley, C. and Houston, A., 2017. Evolution of a long-track violent tornado within a simulated supercell. *Bulletin of the American Meteorological Society*, **98**, 45–68. https://doi.org/10.1175/BAMS-D-15-00073.1

Peters, J.M., Hannah, W. and Morrison, H., 2019a: The influence of vertical wind shear on moist thermals. *Journal of the Atmospheric Sciences*, **76**, 1645–1659. https://doi.org/10.1175/JAS-D-18-0296.1

Peters, J.M., Nowotarski, C.J. and Morrison, H., 2019b: The Role of Vertical Wind Shear in Modulating Maximum Supercell Updraft Velocities. *Journal of the Atmospheric Sciences*, **76**, 3169–3189. https://doi.org/10.1175/JAS-D-19-0096.1

Peters, J. M., C. J. Nowotarski, J. P. Mulholland, and R. L. Thompson, 2020: The influences of effective inflow layer streamwise vorticity and storm-relative flow on supercell updraft properties. *Journal of the Atmospheric Sciences*. https://doi.org/10.1175/JAS-D-19-0355.1.

Przybylinski, R. W. (1995). The bow echo: Observations, numerical simulations, and severe weather detection methods. *Weather and Forecasting*, **10**, 203–218. https://doi.org/10.1175/1520-0434(1995)010%3C0203:TBEONS%3E2.0.CO;2

Púčik, T., Groenemeijer, P., Rýva, D. and Kolář, M., 2015. Proximity soundings of severe and non-severe thunderstorms in central Europe. *Monthly Weather Review*, **143**, 4805–4821. https://doi.org/10.1175/MWR-D-15-0104.1

Rasmussen, E.N. and Blanchard, D.O., 1998. A baseline climatology of sounding-derived supercell and tornado forecast parameters. *Weather and Forecasting*, **13**, 1148–1164. https://doi.org/10.1175/1520-0434(1998)013%3C1148:ABCOSD%3E2.0.CO;2

Rasmussen, E.N. and Straka, J.M., 1998. Variations in supercell morphology. Part I: Observations of the role of upper-level storm-relative flow. *Monthly Weather Review*, **126**, 2406–2421. https://doi.org/10.1175/1520-0493(1998)126%3C2406:VISMPI%3E2.0.CO;2

Rädler, A.T., Groenemeijer, P., Faust, E. and Sausen, R., 2018. Detecting severe weather trends using an additive regressive convective hazard model (AR-CHaMo). *Journal of Applied Meteorology and Climatology*, **57**, 569–587. https://doi.org/10.1175/JAMC-D-17-0132.1

Rotunno, R., Klemp, J.B. and Weisman, M.L., 1988. A theory for strong, long-lived squall lines. *Journal of the Atmospheric Sciences*, **45**, 463–485. https://doi.org/10.1175/1520-0469(1988)045%3C0463:ATFSLL%3E2.0.CO;2

Sherburn, K.D. and Parker, M.D., 2014. Climatology and ingredients of significant severe convection in high-shear, low-CAPE environments. *Weather and Forecasting*, **29**, 854–877. https://doi.org/10.1175/WAF-D-13-00041.1

Sherburn, K.D., Parker, M.D., King, J.R. and Lackmann, G.M., 2016. Composite environments of severe and non-severe high-shear, low-CAPE convective events. *Weather and Forecasting*, **31**, 1899–1927. https://doi.org/10.1175/WAF-D-16-0086.1

Sills, D.M.L., and Joe, P.I., 2019. From Pioneers to Practitioners: A Short History of Severe Thunderstorm Research and Forecasting in Canada, *Atmosphere-Ocean*, **57**, 249–261. https://doi.org/10.1080/07055900.2019.1673145

Smith, B.T., Thompson, R.L., Grams, J.S., Broyles, C. and Brooks, H.E., 2012. Convective modes for significant severe thunderstorms in the contiguous United States. Part I: Storm classification and climatology. *Weather and Forecasting*, **27**, 1114–1135. https://doi.org/10.1175/WAF-D-11-00115.1

Srivastava, R.C., 1985. A simple model of evaporatively driven downdraft: Application to microburst downdraft. *Journal of the Atmospheric Sciences*, **42**, 1004–1023. https://doi.org/10.1175/1520-0469(1985)042%3C1004:ASMOED%3E2.0.CO;2

Taszarek, M., Brooks, H.E. and Czernecki, B., 2017. Sounding-derived parameters associated with convective hazards in Europe. *Monthly Weather Review*, **145**, 1511–1528. https://doi.org/10.1175/MWR-D-16-0384.1

Taszarek, M., and co-authors, 2019: Derecho Evolving from a Mesocyclone—A Study of 11 August 2017 Severe Weather Outbreak in Poland: Event Analysis and High-Resolution Simulation. *Monthly Weather Review*, **147**, 2283–2306. https://doi.org/10.1175/MWR-D-18-0330.1

Taszarek, M., and co-authors, 2020: Severe convective storms across Europe and the United States. Part 2: ERA5 environments associated with lightning, large hail, severe wind and tornadoes. *Journal of Climate*, **33**, 10263–10286. https://doi.org/10.1175/JCLI-D-20-0346.1

Thompson, R.L., 1998. Eta Model storm-relative winds associated with tornadic and nontornadic supercells. *Weather and Forecasting*, **13**, 125–137. https://doi.org/10.1175/1520-0434(1998)013%3C0125:EMSRWA%3E2.0.CO;2

Thompson, R.L., Edwards, R., Hart, J.A., Elmore, K.L. and Markowski, P., 2003. Close proximity soundings within supercell environments obtained from the Rapid Update Cycle. *Weather and Forecasting*, **18**, 1243–1261. https://doi.org/10.1175/1520-0434(2003)018%3C1243:CPSWSE%3E2.0.CO;2

Thompson, R.L., Mead, C.M. and Edwards, R., 2007. Effective storm-relative helicity and bulk shear in supercell thunderstorm environments. *Weather and Forecasting*, **22**, 102–115. https://doi.org/10.1175/WAF969.1

Togstad, W. E., J. M. Davies, S. J. Corfidi, D.R. Bright, and A. R. Dean, 2011: Conditional probability estimation for significant tornadoes based on Rapid Update Cycle (RUC) profiles. *Weather and Forecasting*, **26**, 729–743. https://doi.org/10.1175/2011WAF2222440.1

Trapp, R.J., Stumpf, G.J. and Manross, K.L., 2005. A reassessment of the percentage of tornadic mesocyclones. *Weather and Forecasting*, **20**, 680–687. https://doi.org/10.1175/WAF864.1

Trapp, R.J., Marion, G.R. and Nesbitt, S.W., 2017. The regulation of tornado intensity by updraft width. *Journal of the Atmospheric Sciences*, **74**, 4199–4211. https://doi.org/10.1175/JAS-D-16-0331.1

Trudeau, F., and I. Zawadzki, 1983: On the Influence of the Vertical Wind Structure on Convective Precipitation. *J. Climate Appl. Meteor.*, ***22***, 512–515. https://doi.org/10.1175/1520-0450(1983)022%3C0512:OTIOTV%3E2.0.CO;2

Tsonevsky, I., 2015: New EFI parameters for forecasting severe convection. *ECMWF Newsletter*, No. 144, ECMWF, Reading United Kingdom, 27-32. https://doi.org/10.21957/2t3a904u.

Tsonevsky, I.; Doswell, C.A.; Brooks, H.E. Early warnings of severe convection using the ECMWF extreme forecast index. *Wea. Forecasting* **2018**, *33,* 857–871. https://doi.org/10.1175/WAF-D-18-0030.1

Van Everdingen, E., 1925: The cyclone-like whirlwinds of August 10th 1925. *Verh. K. Akad. Wet. Amsterdam*, **28**, 871–889. https://www.dwc.knaw.nl/DL/publications/PU00015231.pdf

Wakimoto, R. M., and J. W. Wilson, 1989: Non-supercell tornadoes. *Monthly Weather Review*, **117**, 1113–1140. https://doi.org/10.1175/1520-0493(1989)117%3C1113:NST%3E2.0.CO;2

Wegener, A. L., 1928: Beiträge zur Mechanik der Tromben und Tornados. *Meteorologische Zeitschrift*, **45**, 201–214.

Weisman, M.L. and Klemp, J.B., 1982. The dependence of numerically simulated convective storms on vertical wind shear and buoyancy. *Monthly Weather Review*, **110**, 504–520. https://doi.org/10.1175/1520-0493(1982)110%3C0504:TDONSC%3E2.0.CO;2

Weisman, M.L. and Klemp, J.B., 1984. The structure and classification of numerically simulated convective storms in directionally varying wind shears. *Monthly Weather Review*, **112**, 2479–2498. https://doi.org/10.1175/1520-0493(1984)112%3C2479:TSACON%3E2.0.CO;2

Weisman, M.L. and Klemp, J.B., 1986. Characteristics of isolated convective storms. In *Mesoscale meteorology and forecasting*, 331–358. American Meteorological Society, Boston, MA. https://doi.org/10.1007/978-1-935704-20-1_15

Weisman, M.L., 1993. The genesis of severe, long-lived bow echoes. *Journal of the atmospheric sciences*, **50**, 645–670. https://doi.org/10.1175/1520-0469(1993)050%3C0645:TGOSLL%3E2.0.CO;2

Weisman, M.L. and Rotunno, R., 2000. The use of vertical wind shear versus helicity in interpreting supercell dynamics. *Journal of the Atmospheric Sciences*, **57**, 1452–1472. https://doi.org/10.1175/1520-0469(2000)057%3C1452:TUOVWS%3E2.0.CO;2

Wilhelmson, R.B. and Klemp, J.B., 1978. A numerical study of storm splitting that leads to long-lived storms. *Journal of the Atmospheric Sciences*, **35**, 1974–1986. https://doi.org/10.1175/1520-0469(1978)035%3C1974:ANSOSS%3E2.0.CO;2